The MIT Marine Industry Collegium
Opportunity Brief #37

Marine Corrosion and Biofouling

A Project of
The Sea Grant College Program
Massachusetts Institute of Technology
MITSG 84-5

The MIT Marine Industry Collegium

MARINE CORROSION AND BIOFOULING

Opportunity Brief #37

Revised Edition
December 15, 1984

Marine Industry Advisory Services
MIT Sea Grant Program

Cambridge, Massachusetts 02139

Report No. MITSG-84-5
Grant No. NA81AA-D-00069
Project No. A/M-2

This Opportunity Brief and the accompanying workshop held on March 13, 1984 were presented as part of the MIT Marine Industry Collegium Program, which is supported by the NOAA Office of Sea Grant, by MIT and by more than 100 member corporations and government agencies. The workshop was held to provide Collegium members an opportunity to discuss these topics with faculty and students involved in the research outlined herein. The author remains responsible for the conclusions presented herein. The agenda for the workshop is located in the appendix.

The work presented here is part of a larger research program, entitled, The National Sea Grant Corrosion Program. More information about the National Sea Grant Corrosion Program can be obtained by ordering a copy of the Sea Grant Program on Marine Corrosion Final Report - Volume 1 - Technical Summary from the Collegium office. Write to the MIT Marine Industry Collegium, 292 Main Street, Cambridge, MA 02139.

Through Opportunity Briefs, workshops, symposia and other interactions the Collegium provides a means for technology interchange among academia, industry and government for mutual benefit. For more information, contact the Marine Industry Advisory Service at the MIT Sea Grant Program at (617) 253-4434/7092.

Margaret Linskey
December 15, 1984

Table of Contents

1.0 INTRODUCTION

Every year corrosion causes $70 billion in damages in the United States, according to a recent study by the National Bureau of Standards. The report further stated that 15% of those losses could have been avoided by applying known technology. While the study made no attempt to isolate the economic losses associated with seawater corrosion to marine transportation and offshore structures, it seems reasonable to assign at least 10% or $7 billion to marine losses.

It was determined by the NBS that approximately 1/3 of the corrosion that occurs can be attributed to natural processes of thermodynamics and cannot be helped. One-third can be saved by researching better materials and developing new alloys and 1/3 is lost to lack of education on the part of people using corrosive materials. It is believed by corrosion scientists that this latter 1/3 could be prevented if we could educate people to use the corrosion prevention techniques that have been known since 1940, but until recently there have not been economic incentives to do so.

With strong support from the National Sea Grant Office of the United States Department of Commerce, a group of eight marine materials scientists from five universities and one industrial research laboratory have coordinated their efforts to solve selected marine corrosion problems of both practical and scientific importance.

Through consultation with an industry advisory panel, two broad problem areas were selected based on their practical significance to marine-related industries, on the availability of facilities, and on the capabilities and interests of the researchers. The two areas are 1) the relation between calcareous deposits and cathodic protection of structural steel; and 2) the localized corrosion of aluminum and stainless alloys.

The general approach to the two problem areas combined natural seawater testing, electrochemical science, surface science, mathematical modeling and accelerated laboratory testing to better understand the basic processes involved, and to generate data useful to design marine structures.

This Opportunity Brief and the accompanying workshop are part three of an MIT Marine Industry Collegium workshop series highlighting the research of the National Sea Grant Corrosion Program. Figure 1 is an organizational chart of the research projects and principal investigators involved in this program. The first part of the Collegium series focused on Professor Ron Latanision's work at MIT on the corrosion of aluminum in seawater. The second part explored the work of Professors S. Smith, W. Hartt and S. Dunn on marine corrosion and fatigue at the Florida Atlantic University. Finally, this Opportunity Brief discusses a workshop on the marine corrosion research underway at the University of Delaware.

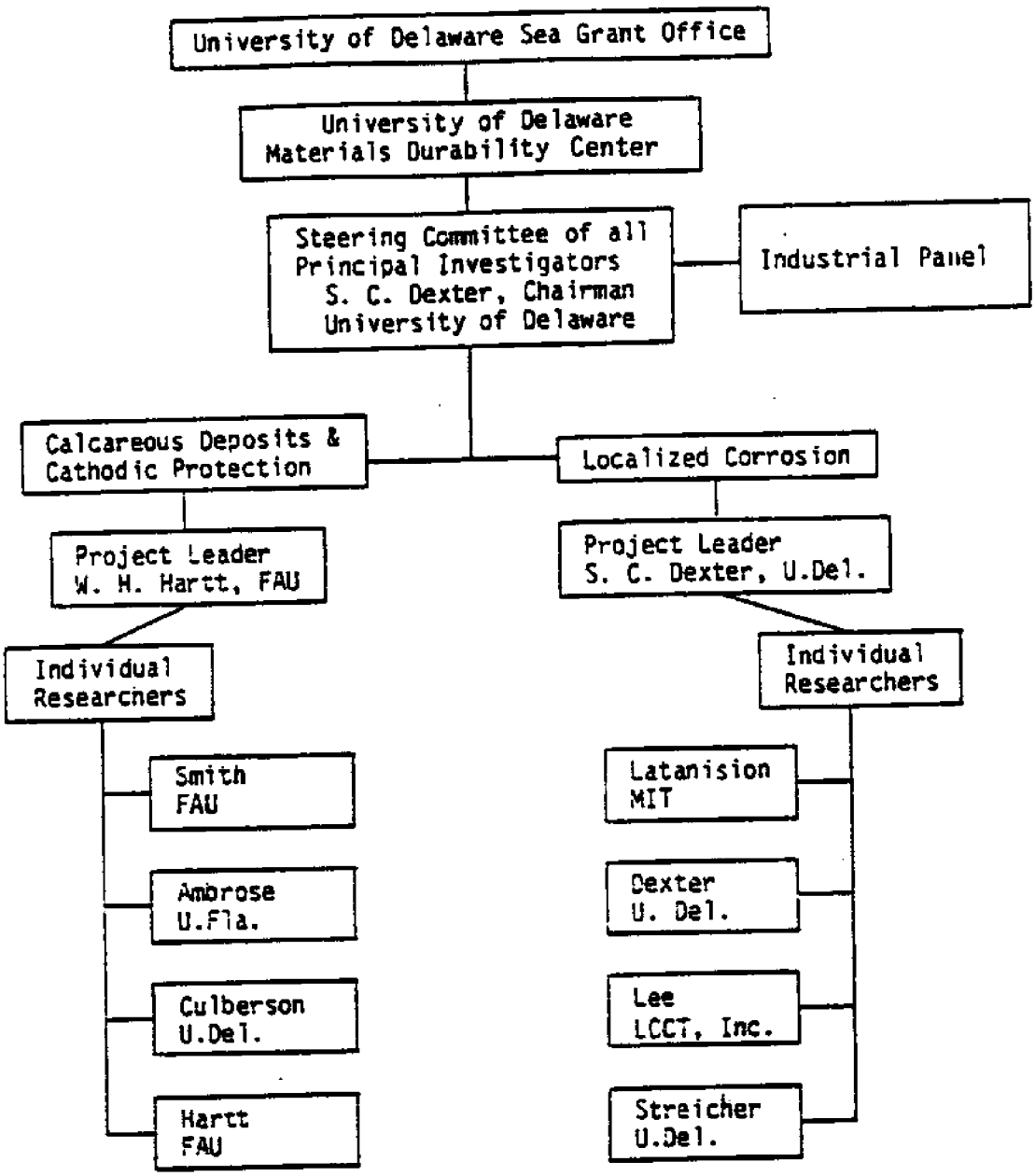

Figure 1: Organizational chart of researcher projects and principal investigators in the National Sea Grant Program.

Professor Stephen Dexter of the University of Delaware College of Marine Studies presented his work on the mechanism of cathodic protection and the effect of water chemistry and velocity of flow on the corrosion of aluminum. Professor Charles Culberson, also of the College of Marine Studies discussed the effect of seawater chemistry on the formation of calcareous deposits during cathodic protection. Professor Michael Streicher of the College of Engineering presented results of recent work on accelerated tests for crevice corrosion of stainless steel alloys in seawater. Finally, James Mihm, a PhD candidate in the College of Marine Studies presented results on the effect of adsorbed organic films on settlement and adhesion of marine larvae. The workshop, Marine Corrosion and Biofouling, took place on March 13, 1984 at the University of Delaware in Newark.

The background presented here is based on interviews with the scientists, on papers given at the National Association of Corrosion Engineers Conference, Corrosion '83 and '84 and on the draft Final Report for the Sea Grant Program on Marine Corrosion (1) and on the presentations given at the workshop.

2.0 THE MECHANISM OF CATHODIC PROTECTION

Introduction

The application of cathodic protection to a metal in a corrosive environment is generally agreed to be beneficial, but there has existed for several decades a disagreement over the electrochemical pathway by which the cathodic protection is achieved. Dr. Stephen Dexter of the University of Delaware has investigated this problem and its implications. The following report is based on his paper presented at the April NASC Corrosion '84 Conference (2) and at an MIT Sea Grant workshop in March, 1984.

Theoretical Background

A uniformly corroding surface, such as plain carbon structural steel in seawater, is thought to have a fairly equal number of anodic and cathodic areas which shift position constantly. As corrosion takes place at anodes only, this produces a relatively uniformly corroded surface. Application of cathodic protection to this surface eliminates the electrochemical potential difference between anode and cathode areas, rendering the surface unipotential and making it behave uniformly as a cathode.

The prevailing theory for explaining the electrochemistry of cathodic protection was proposed in the 1930's by Mears and Brown (3), and Hoar (4). They postulated (in Theory A) that an increase in the applied cathodic current reduces the anodic current density. Enough applied cathodic current reduces anodic currents to zero, in accordance with Kirchoff's current laws, and the entire surface is polarized to the potential of local action anodes. This Theory assumes that the constant movement of anode and cathode areas on the surface is not hindered by the application of a cathodic current, or are there metallurgic constraints which artifically fix their positions on the surface.

LaQue (5) has challenged the prevailing theory by postulating in Theory B that the application of cathodic current progressively reduces the size of the local action anodes rather than reducing anodic current density. He further maintains that the increased cathodic current shifts the mixed potential of the surface toward that of the cathodes, ultimately producing a unipotential surface at the potential of the local action cathodes rather than anodes.

Figures 2.1 and 2.2 illustrate these two theories. An unprotected corroding surface has anode (A) and cathode (C) areas moving freely about as shown in Figures. 2.1a and 2.2a. The anodic current density is

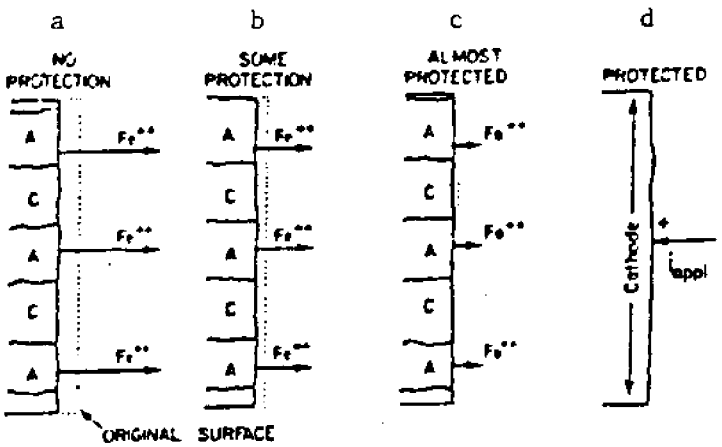

Figure 2.1: Surface profiles for an actively corroding metal as predicted by Theory A, in which the anodic current density is reduced upon application of cathodic protection. A - anodic area, C - cathodic area.

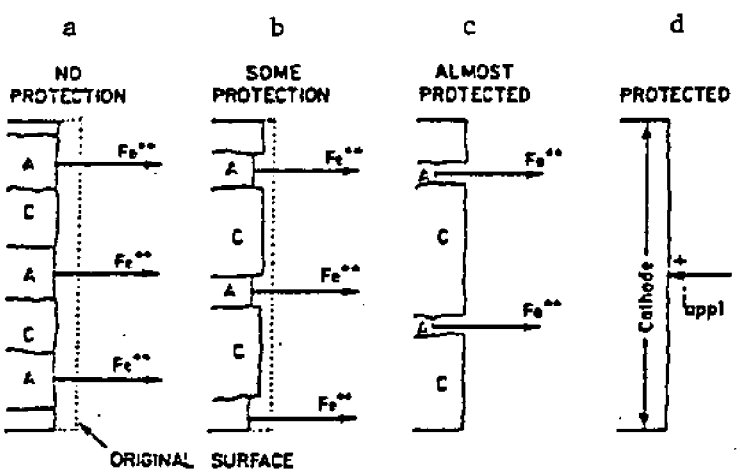

Figure 2.2: Surface profiles for an actively corroding metal as predicted by Theory B, in which the anodic area is reduced but the anodic current density remains unchanged upon application of cathodic protection. A - anodic area, C - cathodic area.

represented by the length of the arrows projecting into the electrolyte. A cathodic current is applied to varying levels of protection in the next three parts of the diagram. In Theory A, the anodic and cathodic areas remain about the same in size while the anodic current density is reduced. In Theory B, the anodic areas shrink with the application of increasing active cathodic current. Theory B predicts that the anodic current density remains the same, while the anodes become very small as cathodic protection is applied. Therefore, according to Theory B, the small anodes on an underprotected surface should not be able to move around freely enough to keep the corrosion uniform, and such an underprotected surface should eventually become roughened or pitted. A surface completely protected over the entire exposure time should have the same morphology according to both theories, but will be at different potentials.

Implications of Research

From the point of view of corrosion science, data collected may clarify the validity of the two theories. Furthermore, the implications in Theory B, that underprotection of a structure may actually induce pitting, is of great interest to corrosion engineering.

Current Investigation

A. The purpose of the work briefly reported here was to investigate the above theories by: 1. direct observations and photographic recording of the behavior of anode and cathode areas on cathodically protected surfaces; 2. investigation of changes of surface roughness as predicted by the two theories.

B. Experimental Technique

1. Testing for Weight Loss:

Long term controlled potential tests were done on samples of AISI 1020 cold rolled steel sheet, cleaned and prepared and inserted into test cell beakers containing natural seawater. The specimens were given various levels of cathodic protection, ranging from not protected to over protected. Voltages were controlled by a series of potentiostats which could set potentials to within one mv and control potential to within 5 mv over the test duration. At the end of 120 days, the steel cupons were removed, photographed, cleaned, rephotographed and weighed. Two additional specimens were tested in an electrolyte of 0.1 M HNO_3 for only 72 hours.

Cathodic polarization curves of the steel cupons in both seawater and acid were measured potentiostatically, starting from the corrosion potential and proceeding in the active (more negative) direction at a rate of 25 mv every five minutes in seawater and 50 mv every five minutes in the acid.

2. Testing for anode and cathode pattern changes:

A parallel set of experiments was performed to observe and to record photographically any changes in the pattern of anode and cathode areas as cathodic protection was applied. Samples of steel and aluminum were abraided and coated with a pH indicator dye which changes color from yellow (acid) to blue (base) in the pH range 6.1-7.7 with a pKa of 7.1. These samples were then immersed into a viscous sodium chloride gel.

The surface of each sample was initially yellow, but within a few minutes after immersion the steel samples began to develop blue and yellow patterns as the anode and cathode areas became defined; it took 15 minutes to 2 hours for these patterns to appear on the aluminum and stainless samples due to the lower corrosion rate. Once a clear pattern was established, cathodic protection was applied either potentiostatically or galvanostatically until complete cathodic protection was achieved as indicated by a completely blue sample surface. The galvanostatic control mode was found optimal in the observation and recording of changes in the surface color pattern. Periodically, throughout the application of the cathodic protection, the surface distribution of anodes and cathodes was recorded photographically.

Experimental Results

A. Cathodic Polarization Curves

Dr. Dexter reports, "Typical cathodic polarization curves are shown for 1020 steel in seawater and in 0.1 m HNO_3 in Figures 2.3 and 2.4 respectively. Corrosion potentials for the steel samples in the recirculated seawater ranged from -500 mV to -650 mV active (negative) to saturated calomel. The curve shown in Figure 2.3 starts at a corrosion potential of -635 mV SCE. The limiting current density for oxygen diffusion was 1.24 $A/_m2$ (0.8 m^A/m^2) and was reached at an applied potential of about -770 mV. The commonly accepted potential for complete cathodic protection of steel in seawater is -800 mV SCE, a potential well within the diffusion limited range of our cathodic polarization curves. Corrosion potentials were commonly more noble (positive) and cathodic current densities 300 or more times larger for steel in 0.1 M HNO3 (Figure 2.4) than they were for the same metal in seawater." (6)

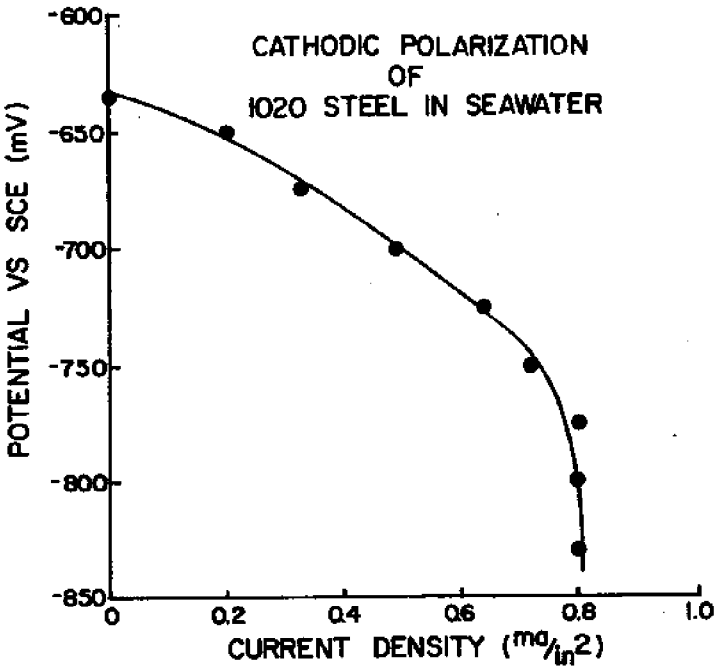

Figure 2.3: Typical cathodic polarization curve for AISI type 1020 steel in seawater. The limiting current density for oxygen diffusion is 0.8 mA/in^2.

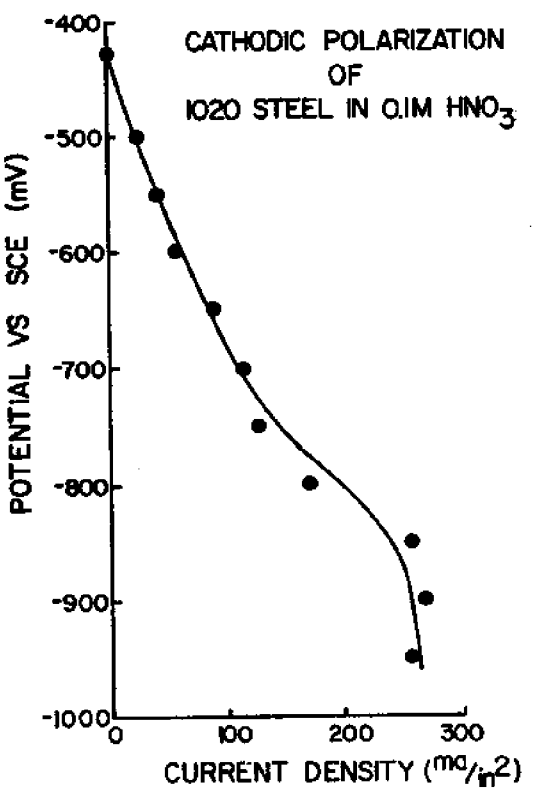

Figure 2.4: Typical cathodic polarization curve for AISI type 1020 steel in 0.1 M HNO_3.

B. Weight loss data

Weight loss data for steel samples are shown in Figure 2.5 for seawater and Figure 2.6 for the acid solution. The samples were held at various potentials within the range of the cathodic polarization curves of Figures 2.3 and 2.4. "Weight loss values of both curves are plotted as a percent of the original sample weight in order to compensate for slight differences in the size of the sample cupons." (7)

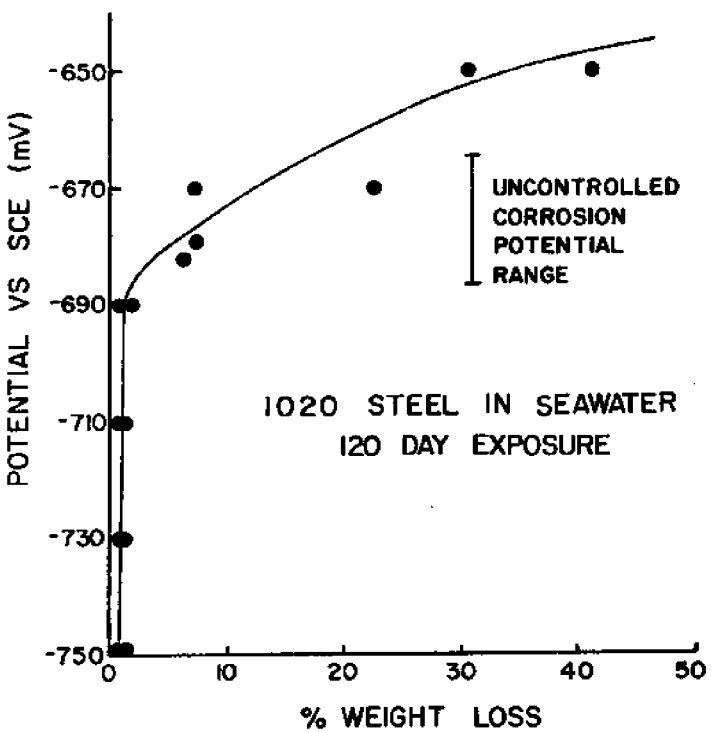

Figure 2.5: Controlled potential as a function of percent weight loss for steel upon a 120 day exposure in seawater. The vertical bar represents the range of corrosion potentials for the freely corroding "control" samples.

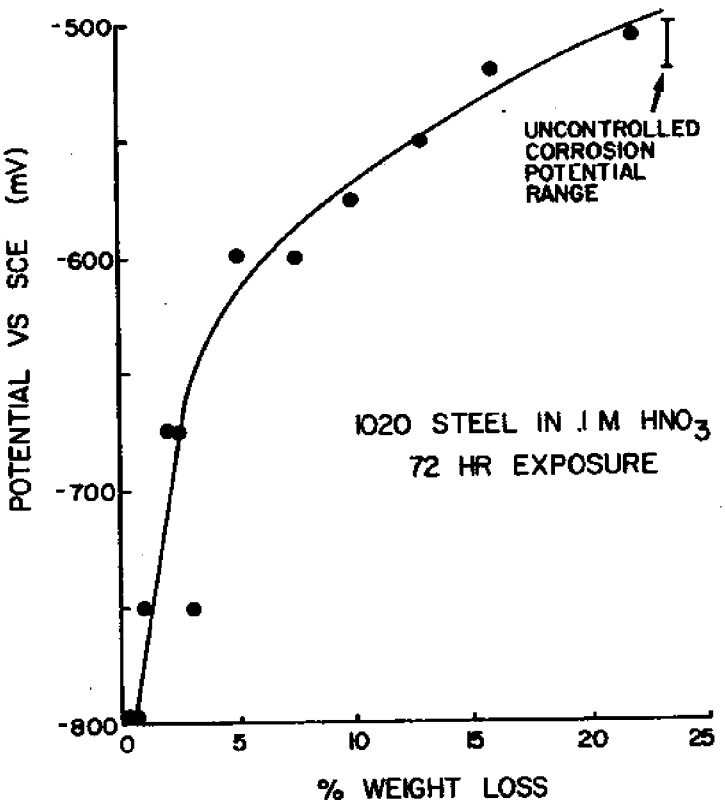

Figure 2.6: Controlled potential as a function of percent weight loss for steel exposed 72 hours in 0.1 M HNO_3.

Two samples in each experiment were left unprotected as "controls." Their original corrosion potentials in seawater were at -670+-5 mV, and their weight loss was plotted at that potential value. The vertical bar on both Figure 2.5 and 2.6 shows the uncontrolled corrosion potential range which was measured daily for these control samples.

Two other samples in seawater were held at -650mV, a potential more positive than their original corrosion potentials. As expected, their weight loss was accelerated.

Several results are of interest. The initial application of cathodic current clearly reduces the scatter in weight loss. Furthermore, the measured weight losses reach very low values by -690 to -700 mV SCE and change very little thereafter at more active potentials. Therefore, according to Dexter's conclusion "complete cathodic protection was achieved in these tests at a potential about 100 mV noble to the generally accepted value, and 60 to 70 mV noble to the value at which the limiting diffusion current density is reached." The data for samples in the acid solution show that by -800 mV, substantial but not yet complete cathodic protection was achieved.

In agreement with Theory A, the weight loss in both the seawater and acid tests was reduced only when the applied current polarized the sample toward the open circuit anode potential. Every time an applied current polarized the specimen toward the cathode potential (the noble direction), an increase in weight loss resulted. This directly contradicts the assertion in Theory B that cathodic protection can be achieved by polarizing to the potential of the local action cathodes.

C. Photographic Evidence

Dexter's study entailed two series of photographs. The first series provided data on surface morphology versus cathodic protection level for the 120 day seawater and 72 hour acid immersion tests. The second series gave data on the surface distribution of anode and cathode areas from the dye tests. We are unable to reproduce those photographs here, but the interested reader can go directly to Dexter's paper. These photographs are of particular interest in the underprotected range of potentials.

C.1 Surface Morphology

The photographs from the long term seawater immersion tests reveal that the anode and cathode areas on the uncontrolled samples were macroscopic and remained stable in location throughout the test period, as shown by the uneven distribution of corrosion products. In contrast, on the controlled potential samples, and at all applied levels, the corrosion products were evenly distributed, the corrosion became more uniform than that on the uncontrolled samples, and there was no evidence of the surface roughening or pitting suggested by Theory B. On the acid immersion samples, the corrosion products were distributed uniformly over the surface of all samples, including the uncontrolled ones.

C.2 Distribution of Anode and Cathode Areas

As cathodic protection was applied to the steel samples, the surfaces in the dye tests usually changed from yellow to blue in a uniform manner, as might be expected on Theory A. For 2024-T6 Aluminum, however, the behavior tended to depend on whether or not the sample had begun to corrode before cathodic protection was applied. If pits were allowed to develop on the surface after immersion in the gel but before applying protection, the anode areas first became better defined and then began to shrink, as implied by Theory B. On the other hand, if protection was applied immediately upon immersion into the gel, the behavior was more like that of the steel samples.

Interestingly, Dexter reported that these two types of behavior could sometimes co-exist on the same sample surface. One region of the surface would change from yellow to blue uniformly, while a neighboring region of the same surface would change by a sweeping motion as the cathode areas grew at the expense of the anode areas.

Discussion

Dexter finally concluded in his March 13 presentation that "For both steel and aluminum surfaces a sequence somewhat intermediate between the classical prediction of Theories A and B was often observed." On most samples, there were regions on the surface where the blue color emerged gradually and others where it swept over a whole region.

Dexter went on to point out that the mixed behavior that was observed does not really contradict Theory A. There is a common misunderstanding that the Mears and Brown Theory requires the anode and cathode areas to remain unchanged in size and shape as cathodic protection is applied. This is not the case, as was clearly stated by Mears in the discussion of their paper. The basic assertions of Theory A are valid whether or not the anode areas change during cathodic polarization.

Dexter found no evidence to support the position taken by LaQue in Theory B that cathodic protection should be applied toward the potential of the local action cathode. The data support the Theory A position that steel in seawater should be polarized toward the local action anode to be protected. Furthermore, there was no evidence to support implication in Theory B that anode areas on underprotected samples behave as if there were no protection, continuing the original rate of penetration until complete protection is achieved.

Conclusions

1. In terms of the size and shape of anode and cathode areas, the behavior of the anodic current density and the potential at which cathodic protection is achieved, the results of Dexter's work are consistent with the Mears and Brown theory and contradict the LaQue theory.

2. The details of the pathway by which cathodic protection is achieved can depend on whether or not corrosion of the surface has begun, and strong anode and cathode areas have developed, before protection is applied.

3. Cathodic protection is achieved by polarizing toward the potential of the local action anodes.

4. Complete cathodic protection of steel in seawater was achieved at a potential of -750 mV SCE.

5. Application of partial cathodic protection always resulted in more uniform corrosion.

6. Partial cathodic protection did not result in surface roughening at magnification up to 50 times. Pitting at remaining anode areas at the unprotected rate did not occur.

7. Polarizing steel in a positive direction from its corrosion potential in seawater always results in an increase in weight loss.

3.0 THE EFFECT OF SEAWATER CHEMISTRY ON THE FORMATION OF CALCAREOUS DEPOSITS DURING CATHODIC PROTECTION

Engineers and scientists concerned with corrosion prevention generally recognize the value of calcareous deposits to effectively and efficiently operate marine cathodic protection systems. These films form on cathodic metal surfaces in seawater, enhancing oxygen polarization and reducing the current density necessary to maintain a prescribed cathodic potential. Even though calcareous deposits have been generated via cathodic protection for years, little is known about the delicate relationship between deposit properties and the conditions under which they form.

In shallow depths diver inspection of cathodic protection systems on offshore structures is extremely reliable. Through regular inspection anode deterioration can be carefully watched. Consequently, anode replacement and current density control are relatively easy. Now that offshore structures are being placed in deeper, colder waters, diver inspection is not only unsafe but is extremely expensive. Therefore, much of the deep ocean structure inspection is now being done by remotely operated vehicles and manned submersibles.

Knowledge of how the ocean environment and chemistry affect cathodic protection systems is equally important as developing accurate inspection and monitoring technology. Until Charles Culberson of the University of Delaware worked out the effect of seawater temperature, pressure and pH on cathodic protection, no one knew why more protection was needed in lower temperatures and at high pressure, for example.

Eventually, the findings of the National Sea Grant Marine Corrosion team will be used to help determine the appropriate amount of protection needed for structures at specific sites.

Culberson has spent the past two and a half years studying the effects of pH, oxygen and temperature on the formation of calcareous deposits. His earlier work on the effect of seawater pH and oxygen content is described below. At the March 13 workshop Culberson presented the results of this past year's research on the role temperature plays in the formation of calcareous deposits.

Culberson's objective was to better understand the fundamental properties of calcareous deposits including their chemical structure, formation rate and effective resistance, as a function of electrochemical, chemical and physical variables of exposure. Such variables include current density and potential, pH, water temperature, seawater chemistry and hydrodynamic flow.

The overall goal of Culberson's research is to provide data which can be used to select the most economical conditions for cathodic protection of steel in seawater. Wolfson and Hartt of the Florida Atlantic University have shown that for a flat steel plate, the long term current requirements for cathodic protection are actually less at -1.04 volt versus a saturated calomel reference electrode than for an applied potential of -.90 volt. The effect of applied potential on the current density will be investigated in further studies.

3.1 Experimental Procedure

The experiments that are discussed below were conducted at the College of Marine Studies at the University of Delaware. To achieve uniform flow characteristics, a rotating cylinder electrode was used. The cylinder was chosen because it has a large surface area, was easy and inexpensive to assemble and it yielded reproducible hydrodynamics. The corrosion cell itself is a 2.5 liter glass beaker which is 5" wide and 12 " high. The cell was filled with 2 liters of test solution (NaCl or seawater) at the beginning of each experiment. Dissolved oxygen concentrations were measured with an oxygen electrode. The pH was measured with a pH electrode standardized on the National Bureau of Standards pH scale. The experiments were done from one to two weeks each at $3^{\circ}C$ and at $25^{\circ}C$.

The reactions which take place at the steel-seawater interface during cathodic protection of steel in seawater follow.

1. Oxygen Reduction:

$$O_2 + 2H_2 + 4_e = 4OH^-$$

2. Precipitation:

$$Ca^{2+} + CO_3^{2-} = CaCO_3$$

$$Mg^{2+} + 2OH^- = Mg(OH)_2$$

The following discussion of Culberson's work is based on a paper which was given at the National Association of Corrosion Engineers: "Corrosion 83", paper #61. (8)

"Studies of the properties of calcareous deposits formed during the cathodic protection of steel in seawater have concentrated on the effects of applied potential, current density and flow. Some work has been done on the effects of environmental variables such as dissolved oxygen, pH, and temperature on the properties of calcareous deposits. These environmental parameters can affect the pH and thus the solubilities of $CaCO_3$ and $Mg(OH_2)$ at the steel-seawater interface." (9)

3.2 Effect of O_2

The effect of oxygen on current density during cathodic protection of steel in sodium chloride is shown graphically in Figure 3.1.

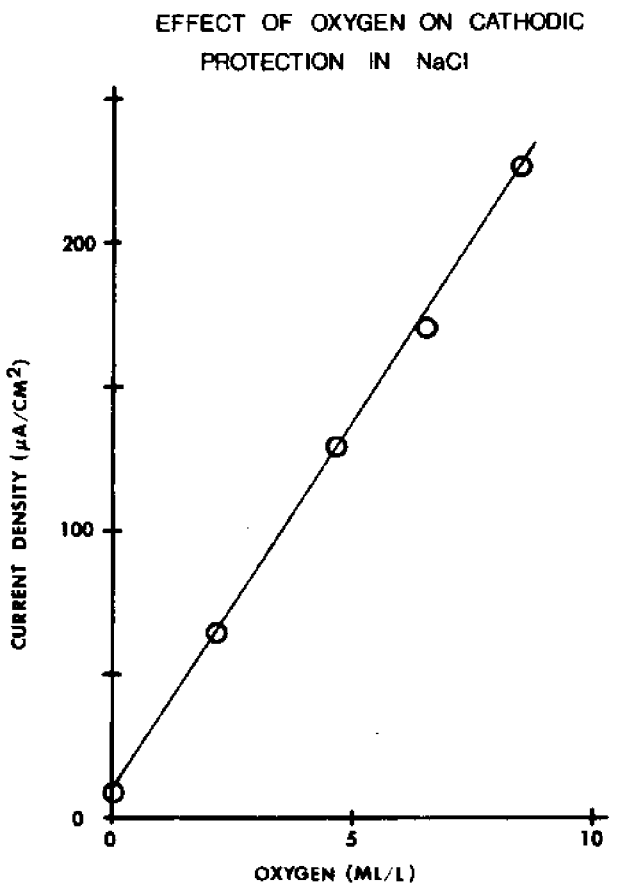

Figure 3.1: Effect of oxygen on current density during cathodic protection of steel in sodium chloride (0.50 NaCl + 0.0027 NaHCO). Temperature = 25°C; pH = 8.3; potential = 0.90 volt; rotation speed = 88 rpm.

The temperature was 25°C, pH was at 8.3 the potential was -0.9 volt and the rotation speed was 88 rpm. These measures show a linear relationship between the dissolved oxygen concentrations and the current density required for cathodic protection.

Figure 3.2 portrays the effect of oxygen and pH on current density during cathodic protection of steel in seawater of 30% salinity.

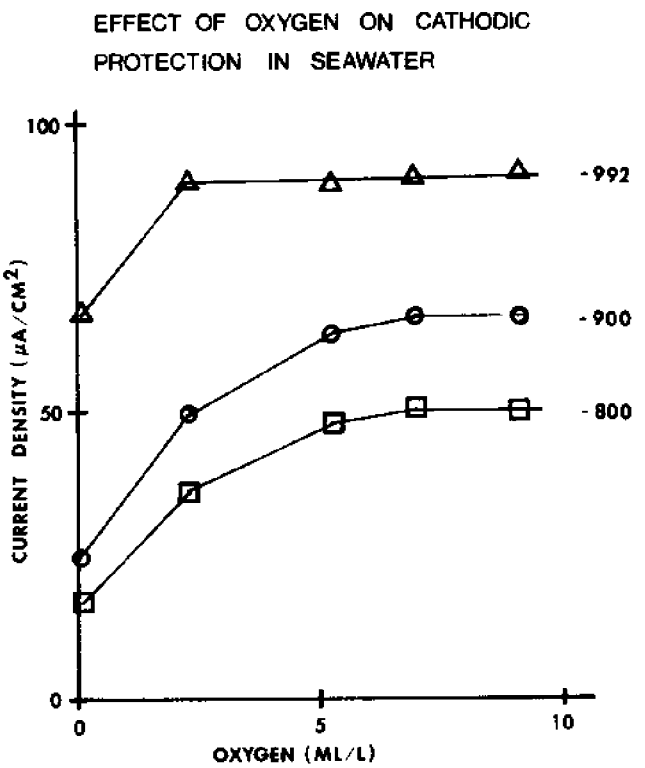

Figure 3.2: Effect of oxygen on current density during cathodic protection of steel in seawater of 29.7% salinity. Temperature = 25°C; pH = 8.2; potentials = -0.80, -0.90, -0.992 volt; rotation speed = 1.05 rpm.

The current in this experiment was measured at three potentials (-99, -800, -992 mv). In contrast to the linear relationship between current density and dissolved oxygen concentration in 3% NaCl and in seawater, the experiment depicted in Figure 3.2 found that although the current density increased with increasing oxygen concentration at low oxygen concentrations, it remained constant or decreased at oxygen greater than air saturation.

3.3 Effect of pH

Figure 3.3 shows the effect of solution pH on current density during cathodic protection of steel in seawater of 29.7% salinity with a temperature of 25°C, oxygen of 4.9 ml. These data demonstrate that current density decreases as the solution pH increase. This is probably due to the increased concentrations of carbonate and hydroxide ions in solution which cause $CaCO_3$ and $Mg(OH)_2$ to be less soluble at the steel-water interface.

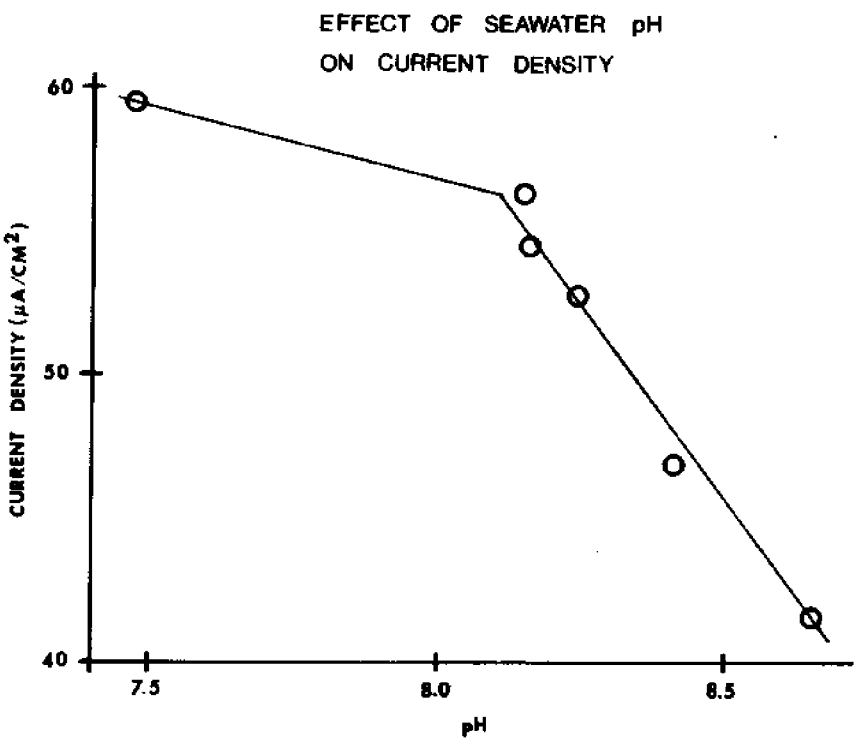

Figure 3.3: Effect of seawater pH on current density during cathodic protection of steel in seawater of 29.7% salinity. Temperature - 25°C; oxygen = 4.9 ml O_2/liter; potential = 0.90 volt; rotation speed = 89 rpm.

The results of a study of the effect of dissolved inorganic carbon on cathodic protection are summarized in Table 3.1. The decrease in current density at high pH could be due to several factors since the concentrations of hydroxide, biocarbonate, carbonate, and total dissolved inorganic carbon ($CO_2 + HCO^- + CO^-$) all change with the pH. The negative linear correlation between current density and the carbonate ion concentration shown in Figure 3.4 suggests that increased carbonate ion concentration in solution enhances the precipitation of $CaCO_3$ at the steel-water interface and thus reduces the current density.

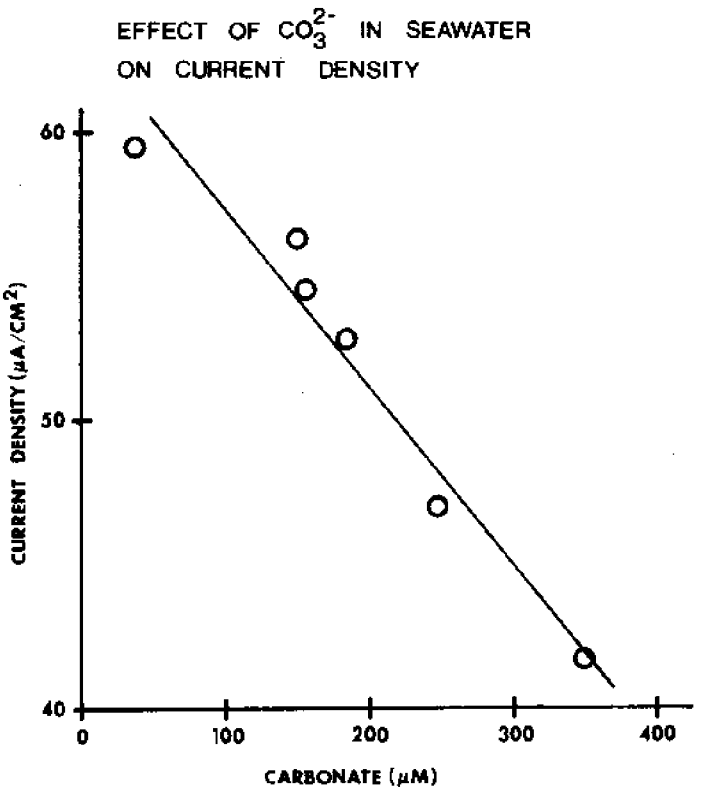

Figure 3.4: Correlation of current density and seawater carbonate ion concentration. Same conditions as Figure 3.3.

There is a positive linear correlation between current density and bicarbonate ion concentration, and between current density and the concentration of total dissolved inorganic carbon. However, because of the positive correlation, the lowest current densities occur at the lowest concentrations of these two parameters. Therefore, the concentrations of bicarbonate and total carbon do not seem to control the current density.

Table 3.1

The Effect of Dissolved Inorganic Carbon on Cathodic Protection

pH	TCO_2	HCO_3	CO_3	pCO_2	aOH x 10^6
	----------(micromolar)-------			(ppm)	
8.16	1788	1618	158	402	1.4
8.65	1502	1151	348	92	4.5
8.41	1655	1405	245	196	2.6
8.24	1749	1557	183	322	1.7
7.47	2022	1914	38	2332	0.3
8.15	1792	1625	155	413	1.4

Note: Acid-base speciation during cathodic protection of steel in seawater. Salinity = 29.73/100, temperature = 25°C. Dissociation constants of carbonic acid were taken from Millero (7). TCO_2 is total inorganic carbon dioxide.

Source: Culberson, C. Corrosion '83 Paper #61, NACE, April, 1983

3.4 Effect of Temperature:

The effect of temperature on calcareous deposit formation was studied during 1983. Preliminary studies indicate that current density necessary for polarization to a given potential in calcium ion free synthetic seawater was greater at 25°C than 3°C. For natural seawater, where calcareous deposits may form, current density was less at 25°C. Apparently the lower temperature inhibits calcareous deposit formation.

Figure 3.5 shows the results of an experiment where the time variation of current density during cathodic protection of steel in seawater is measured. The temperature was 3°C and 25°C, potential was -0.9 volts, the rotation speed was 50 rpm, air saturation.

The experiment began at 3°C. The figure shows how the current density decreases the first day or so, and then levels off. At the end of day 6, the temperature is increased to 25°C. The results show that current density decreases with time. Decreases in current density generally indicate increases in calcareous deposits.

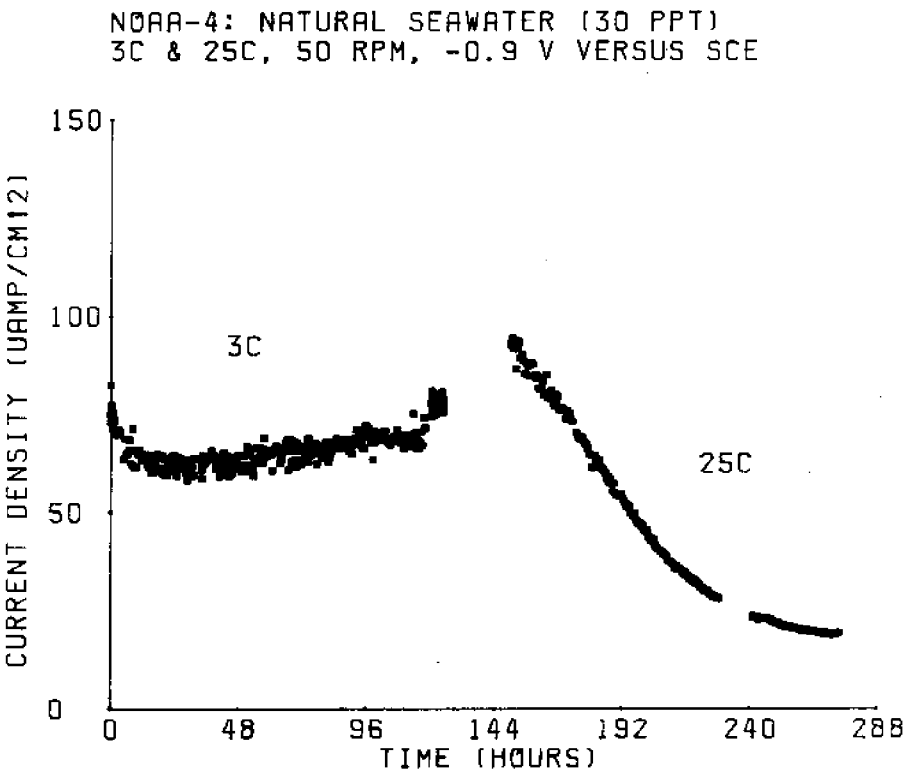

Figure 3.5: Time variation of current density during cathodic protection of steel in seawater of 31% salinity. Temperature = 3°C and 25°C; potential = -0.90 volt; rotation speed = 50 prm; air saturation; experiment NOAA-4.

This data confirms what happens in nature: that it is difficult to precipitate calcareous deposits at low temperatures.

Culberson postulates that temperature must effect the kinetics of precipitation at the steel surface. Thus researchers have more motivation to learn more about exactly what happens at the steel surface.

Figure 3.6 shows the results of an experiment to investigate the effect of temperature on calcareous deposit formation without calcium or magnesium in the solution. The electrode was placed in a sodium chloride plus sodium bicarbonate solution. In this figure current density is plotted as a function of rotation. In a system where calcareous deposits are not formed the current densities at high temperature are higher than those at low temperatures.

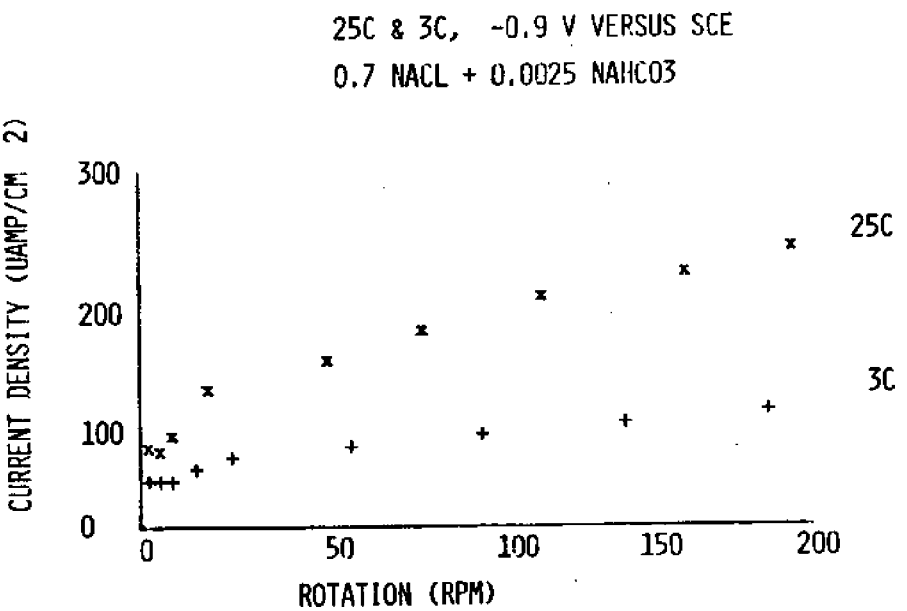

Figure 3.6: Effect of rotation speed on current density during cathodic protection of steel at 25°C and 3°C. Solution composition 0.70 NaCl + 0.0025 $NaHCO_3$; potential = -0.90 volt; air saturation; experiment NOAA-6.

The results were exactly opposite in seawater. There are higher current densities of 3°C then at 20°C simply due to the presence of a deposit. Calcium and magnesium were removed from the test solution to isolate the reactions in the format of calcareous deposits. The role these two play in the formation of calcareous deposits is essential to understanding the entire process.

Figure 3.7 shows the effect of magnesium on cathodic protection of steel in synthetic seawater. The solution composition is .50 NaCl + 0.03 Na_2SO_4 + .0025 $NaHCO_3$ + .05 $MgCl_2$. The temperature is 25°C, the potential is -.90 volt and the rotation speed is 50 rpm with air saturation. The synthetic seawater has everything in it except calcium.

The experiment mentioned above was to see what kind of a deposit one could get from magnesium hydroxide, and to see how effective magnesium hydroxide is in forming a deposit on the steel surface. The question remains, what forms first, magnesium hydroxide or a mixture of hydroxide and carbonate. Hartt and Smith at the Florida Atlantic University are looking at the process of initial formation of calcareous deposits.

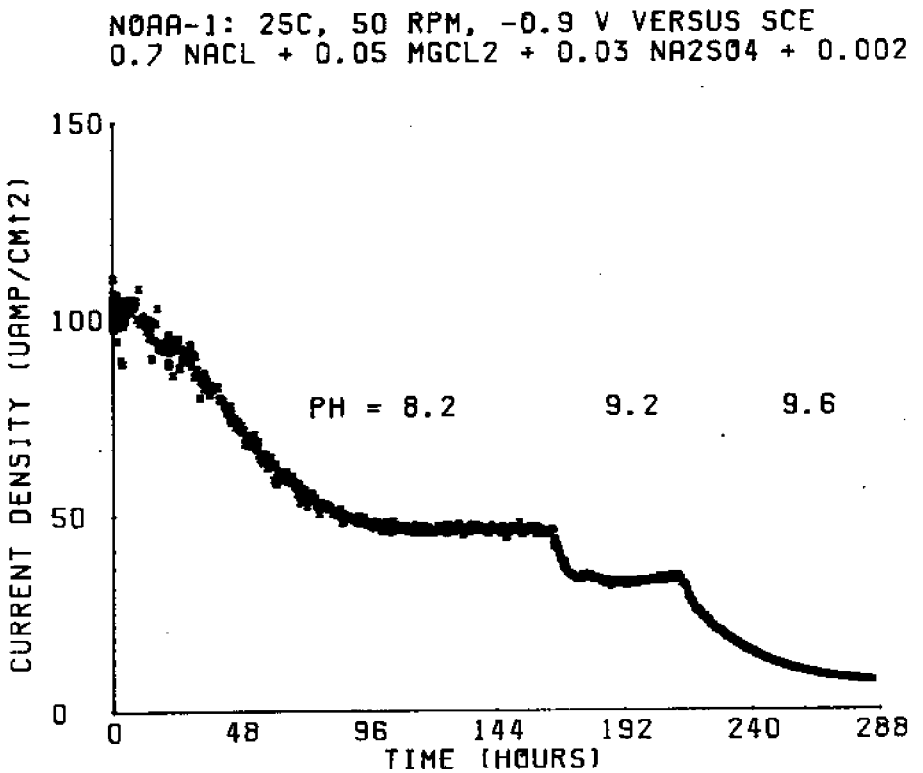

Figure 3.7: The effect of magnesium on cathodic protection of steel in synthetic seawater. Solution composition 0.50 NaCl + 0.03 Na_2SO_4 + 0.0025 NaHCO + 0.05 $MgCl_2$; temperature = 25°C; potential = -0.90 volt; rotation speed = 50 rpm; air saturation.

Now that more is known about the variables affecting calcareous deposit formation seawater the next step is to fit this data into a model. Culberson et al at the University of Delaware intend to build a model that will allow predictions of calcareous deposit formation given pH, water chemistry, temperature, current density and potential and hydrodynamic flow. When the model is developed it will help design engineers specify the amount of cathodic protection that is necessary and economical to protect a structure in a specific location.

3.5 Conclusions

Culberson's experiments lead to the following conclusions:

1. The presence of magnesium ion in seawater markedly increases current requirements for cathodic protection because magnesium inhibits the precipitation of $CaCO_3$ at the steel-water interface. See Figure 3.7.

2. The current density does not increase linearly with increasing oxygen concentrations in seawater, but reaches a plateau at oxygen concentrations greater than air saturation.

3. Current requirements for cathodic protection decrease at high solution pH, and a linear relationship occurs between current density and the seawater carbonate ion concentration.

4. Preliminary studies on the effect of temperature on formation of calcareous deposits indicate that current density necessary for polarization to a given potential in a calcium ion free synthetic seawater was greater at 25°C than at 3°C. For natural seawater, where calcareous deposits may form, current density was less at 25° C. The lower temperature inhibits calcareous deposit formation.

4.0 THE EFFECT OF SEAWATER CHEMISTRY AND FLOW ON CORROSION OF ALUMINUM

Recent work by Steve Dexter on the effect of seawater chemistry and velocity flow on aluminum corrosion is part of a larger effort by others on localized corrosion. (See Figure 4.1.) Much of the research is related to Latanision's work at the MIT Materials Science and Engineering Department on the corrosion of aluminum in seawater. (10) The objectives of Latanision's project were to clarify the roles of magnesium, copper, organic films and velocity of flow on the pitting corrosion of aluminum-magnesium alloys in seawater, so that these variables can be included in the modeling and predictive work being addressed by others in the program.

The following description of Latanision's work on how aluminum corrodes in seawater provides background for the discussion of Dexter's research on the effect of seawater flow and chemistry on the corrosion of aluminum. Latanision found that the presence of magnesium on an aluminum surface in aerated seawater influences the cathodic reaction during corrosion. The behavior of pure aluminum and aluminum-magnesium alloys in natural seawater could not be reproduced in sodium chloride solutions in the laboratory until bicarbonate and magnesium were introduced into the system. Bicarbonate dissociates into carbonate ions and dissolved molecular carbon dioxide, allowing laboratory simulation of the carbonic acid system which controls the pH of natural seawater.

Latanision conducted an experiment in which enough EDTA (ethylene diamine tetraacetic acid) was added to the solution containing the electrode to complex all magnesium present during that experiment. 1200 ppm Mg were added at a time, -15 minutes, and gave the usual noble shift in corrosion potential.

"According to the reaction below, the proposed role of magnesium is to act as a catalyst for the reduction of percarbonic acid, an intermediate species in the seawater carbonic acid system according to:

$$H_2CO_4 + 2H^+ + 2e^- \xrightarrow{MG^{++}} CO_2 + 2H_2O.$$

The above reaction would provide another reduction current to depolarize the cathode in natural seawater but not in sodium chloride solutions. This was viewed as one possible reason why seawater is often observed to be more corrosive than 3 to 3.5% sodium chloride." (11)

Based on this work, Dexter considered different aspects of the role of magnesium and asked whether other divalent cations present in seawater can produce a similar effect.

The principal factors affecting cathodic reduction of oxygen on aluminum in seawater are oxygen concentration, temperature, pH and ionic species. These parameters directly affect corrosion potential and/or the shape of the cathodic polarization curve.

4.1 Experimental Techniques

The following experimental details introduce the research method used by Dexter.

Electrodes were prepared identically in order to achieve uniformity of the aluminum surfaces prior to testing. Specimens were abraded with 600 grit emery paper, degreased with acetone, pickled to 20% nitric acid, dipped in 1M sodium hydroxide and rinsed in distilled water. Electrodes were then aged for 1 hour in room temperature distilled water, prior to immersion in the test cell. After both pickling and aging, the specimens were examined at 25x in a stereomicroscope. Those with pits, significant surface irregularities, and/or crevices at the teflon interface were reabraded, repickled, and reexamined.

The seawater used in these experiments was full strength clean Atlantic Ocean surface water (salinity from 32 to 34 parts per thousand) collected in 55-liter polyethylene jugs at two to three week intervals from 40 to 100 miles off the mouth of Delaware Bay. The water was continuously aerated while stored in the laboratory. Before use, it was passed through glass fiber and 0.2 micrometer membrane filters to remove detritus and marine microorganisms.

The temperature of the test cell was controlled by pumping precooled alcohol through a glass cooling coil inserted into the electrolyte. Temperature control was achieved to $\pm$ 0.5°C over the temperature range 4 to 25°C. The pH of test solutions was controlled to better than $\pm$ 0.05 pH units by adding 0.01N HCl or NaOH to sodium chloride solutions, or by varying the CO_2 partial pressure in natural seawater. Electrolyte pH was monitored with a Fisher Accument digital pH meter. Dissolved oxygen was controlled by varying the oxygen partial pressure and was measured in solution using a YSI Model 57 oxygen meter calibrated by the Winkler titration method. Cathodic polarization experiments were conducted using standard potentiostatic techniques. A freshly pickled and aged electrode was allowed to reach steady state (usually within 45 to 60 minutes) in a 1000 ml six-neck polarization flask containing the test electrolyte.

Flow of electrolyte past the specimen surface was achieved either by varying the rate of stirring in the cylindrical polarization flask by a magnetic stirrer, or by varying the flow rate in a specially constructed flow-through system using the tubular electrodes. (See Figures 4.1 and 4.2). Quantitative control of flow speed and flow character (i.e., laminar or turbulent) were possible only in the flow-through system. The electrodes for the flow-through system, however, were time consuming to prepare, and limited the amount of data taken with that system. For this reason, the supplementary data were obtained by varying the stirring rate in the polarization flask from zero (quiescent conditions) to 1200 rpm.

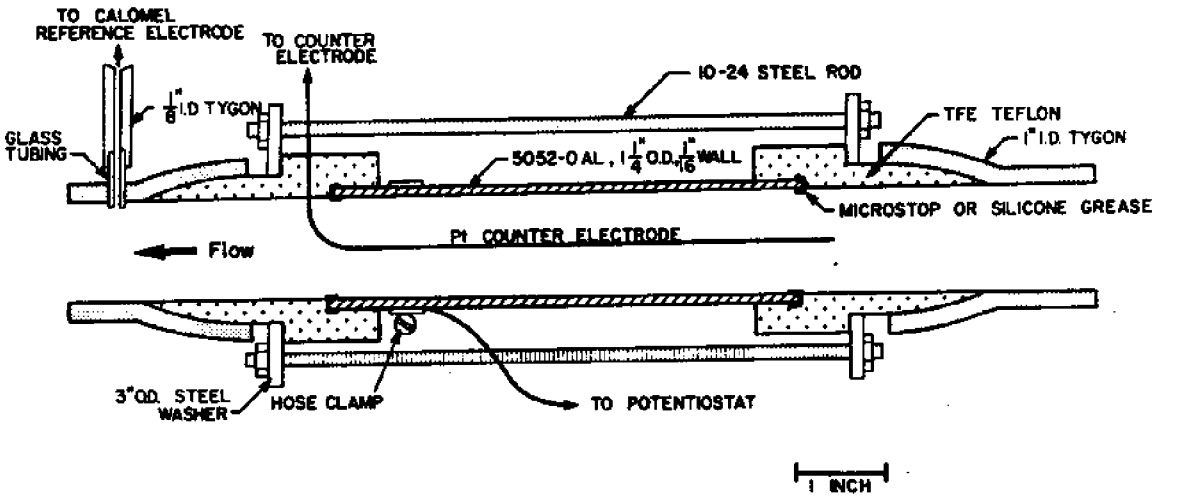

Figure 4.1: The Electrochemical Test Section in the Flow Through System.

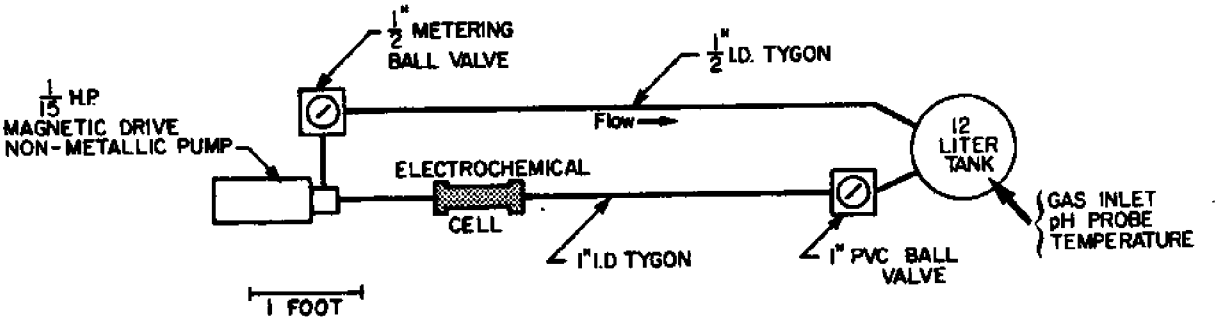

Figure 4.2: Schematic Diagram of Recirculating Flow Through System for Flow Speed Measurements.

To minimize their influence on the hydrodynamics of flow, the pump and metering valve were placed downstream of the electrochemical test section. The flow speed was measured volumetrically by disconnecting the Tygon tubing from the inlet reservoir bulkhead fitting and allowing the water to discharge through an identical fitting at the same pressure head as provided by the reservoir. The flow character was determined both by theoretical calculations and flow visualization experiments in the test section. The critical Reynolds number for the laminar to turbulent transition is 2000-4000 for tubing. For the flow-through electrode this corresponds to 7-14 cm/sec. Mean flow rates ranged from 0.5 to 70 cm/sec and should therefore include laminar, transition, and turbulent flow. This was confirmed by pitot tube measurements and observations of suspended threads with a glass tube replacing the aluminum electrode in the test section. (12)

4.2 The Magnesium Effect

Why the magnesium effect tends to disappear with time is not yet understood. The disappearance is apparently not due to a complexation type of phenomenon because these occur over fractions of a second, whereas the magnesium effect takes tens of hours to disappear. Changes in the passive film over a period of hours are probably involved in the disappearance of the magnesium effect, although the details of the changes involved are not clear. Figure 4.3 illustrates how the magnesium effect decreases with time. Figure 4.4 shows how the current potential of pure aluminum changes with time.

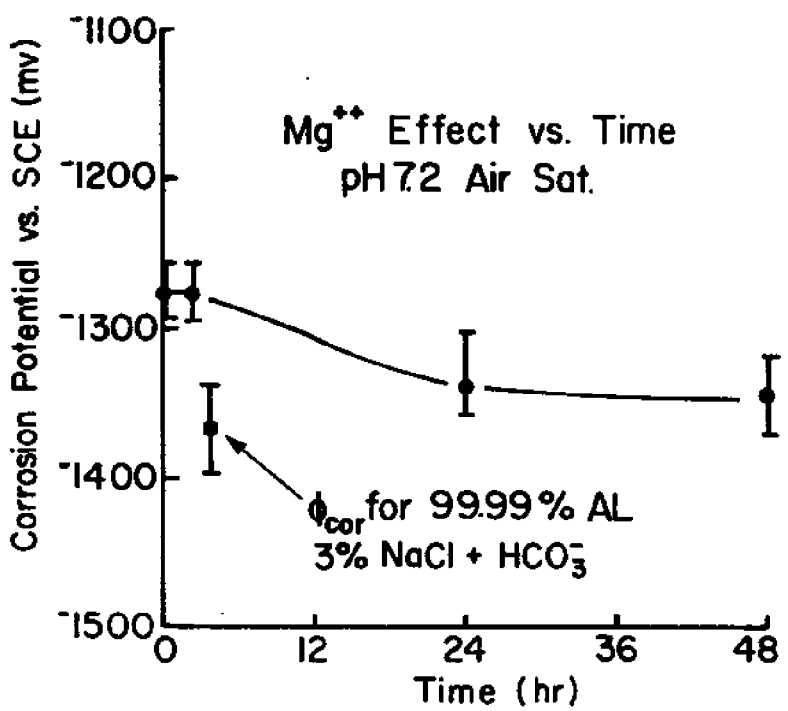

Figure 4.3: Decay of Magnesium Effect with Time. The data point indicated by the arrow represents the corrosion potential prior to addition of magnesium.

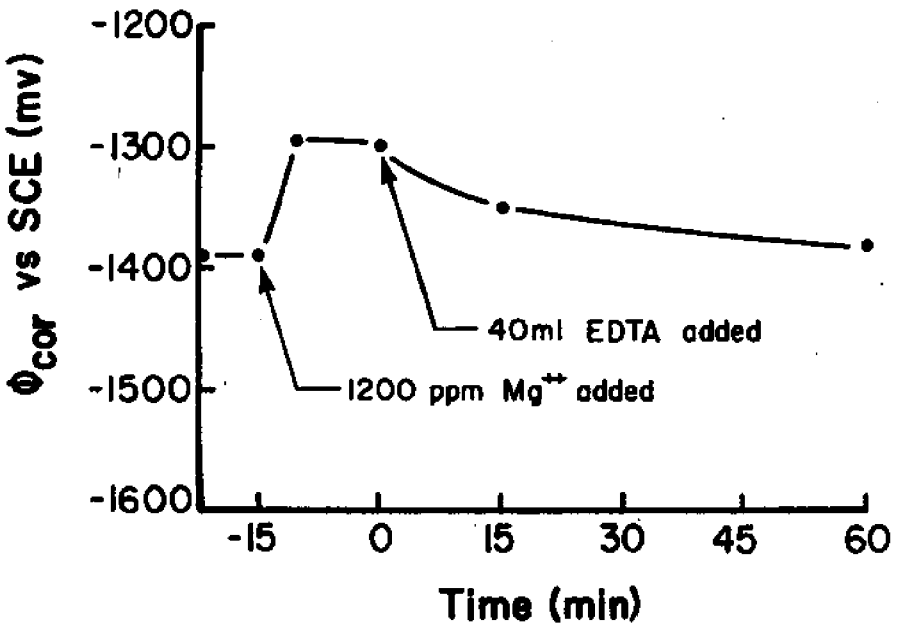

Figure 4.4: Corrosion Potential of Pure Aluminum as a Function of Time Upon Adding Magnesium to the Solution and Subsequently Complexing the Magnesium with Disodium EDTA.

Magnesium clearly plays a role in the cathodic reactions on aluminum in seawater, but it would probably be a mistake to assign too much practical significance to that role. The effect appears to be important only while the passive film is becoming established. Since the effect tends to make the corrosion potential more noble, and since it is maximized at low pH (7.2 to 7.5), it may have some practical impact on initiation of pitting during the first day or so that an aluminum structure is exposed in the deep ocean. Magnesium is less likely to have an effect in surface waters where the pH is greater than 8, and it certainly does not play nearly as significant a role as the chloride ion. Figure 4.5 shows polarization curves of magnesium in seawater with the addition of aluminum and Sr#.

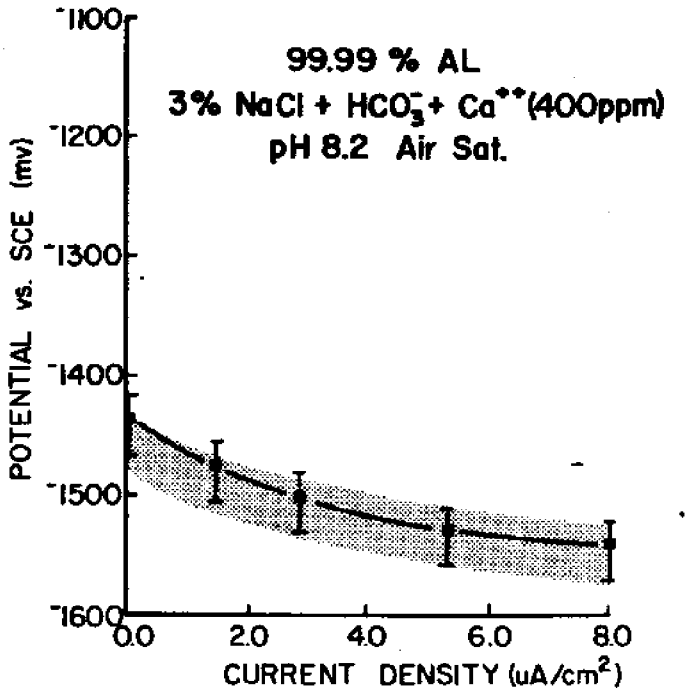

Figure 4.5: Cathodic Polarization of Pure Aluminum in 3% NaCl + HCO_3 at pH 9.2. Polarization curves are consistent with addition of calcium and Sr#.

4.3 Effect of Flow

An increase in the speed of flow past the surface always had two effects in the tests. First, it shifted the corrosion potential in the active direction, which agrees with previous work (13) on aluminum alloy 5456 in high velocity seawater flows. Second, it decreased the initial slope of the cathodic polarization curve. Under surface water conditions where the pH is greater than 8, the corrosion potential effect always predominated. This test predicts that the increase in flow speed normally associated with tidal and wind driven currents in coastal and estuarine waters should lead to less corrosive conditions than those in stagnant water. Although previous experience shows that a continuous flow of about 2 meters/sec is necessary to suppress pitting altogether, these results indicate that even small flow speeds exert some benefit.

The flow was turbulent and highly erratic due to vortex shedding from the gas bubbler, pH electrode and counter electrodes protruding into the

flow. Thus the reason for scattering in the data shown in Figure 4.6. Regardless of the scatter there is a general trend of a decrease in corrosion potential with decreasing pH.

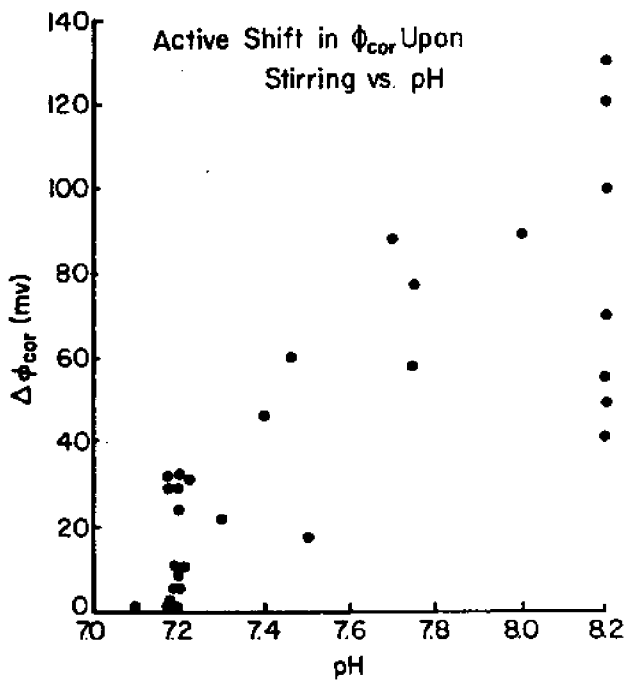

Figure 4.6: Effect of stirring rate on polarization flask on cathodic polarization of alloy 5052 under simulated deep ocean conditions.

Increasing the flow speed gives an increase in the active shift in corrosion potential of alloy 5052 as shown in Figure 4.7 for a pH of 7.5. This part of the experiment shows less scatter because it was done with the flow-through system in which hydrodynamics are controllable. Figure 4.8 illustrates how the corrosion potential changes linearly with the logarithm of the flow speed over the range from 1 to 70 cm/sec.

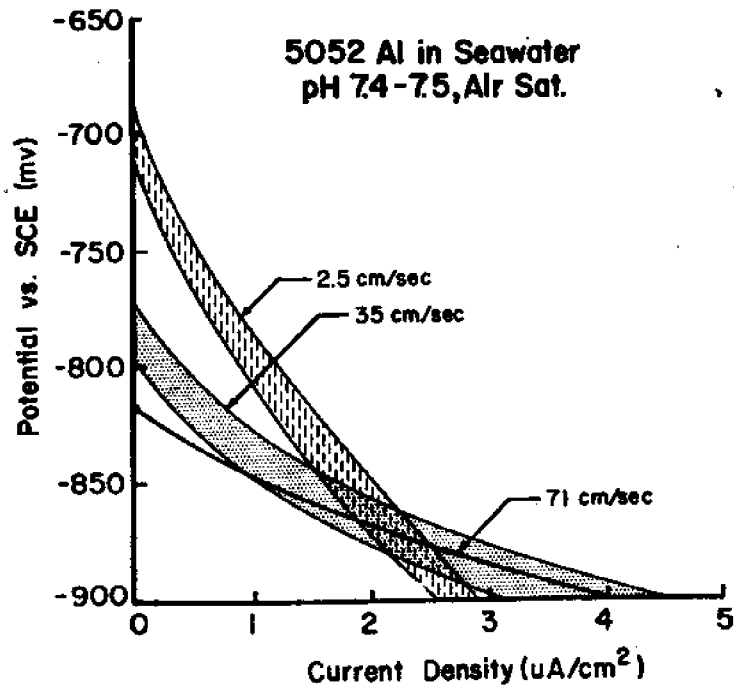

Figure 4.7: Change in corrosion potential of alloy 5052 upon stirring at 1200 rpm in the polarization flask as a function of pH.

Finally, the lack of any systematic variation of cathodic behavior with flow speed under simulated deep ocean conditions as seen in Figure 4.9. This figure indicates that previous concern over the possibility of triggering a set of highly corrosive conditions in the deep ocean by an increase in flow speed probably was unnecessary. The concern originally arose in the Ocean Thermal Energy Conversion Program where deep ocean water might be passing through aluminum condenser tubing at an elevated velocity. The lack of response to flow demonstrated in Figure 4.9 is attributed to sluggish reaction kinetics at the low temperature. The data indicate that under the short time period and the condition in the laboratory tests, flow had little effect on the corrosion process. However, longer time periods or intermediate temperatures in the 10°to 15° C range might still be cause for concern.

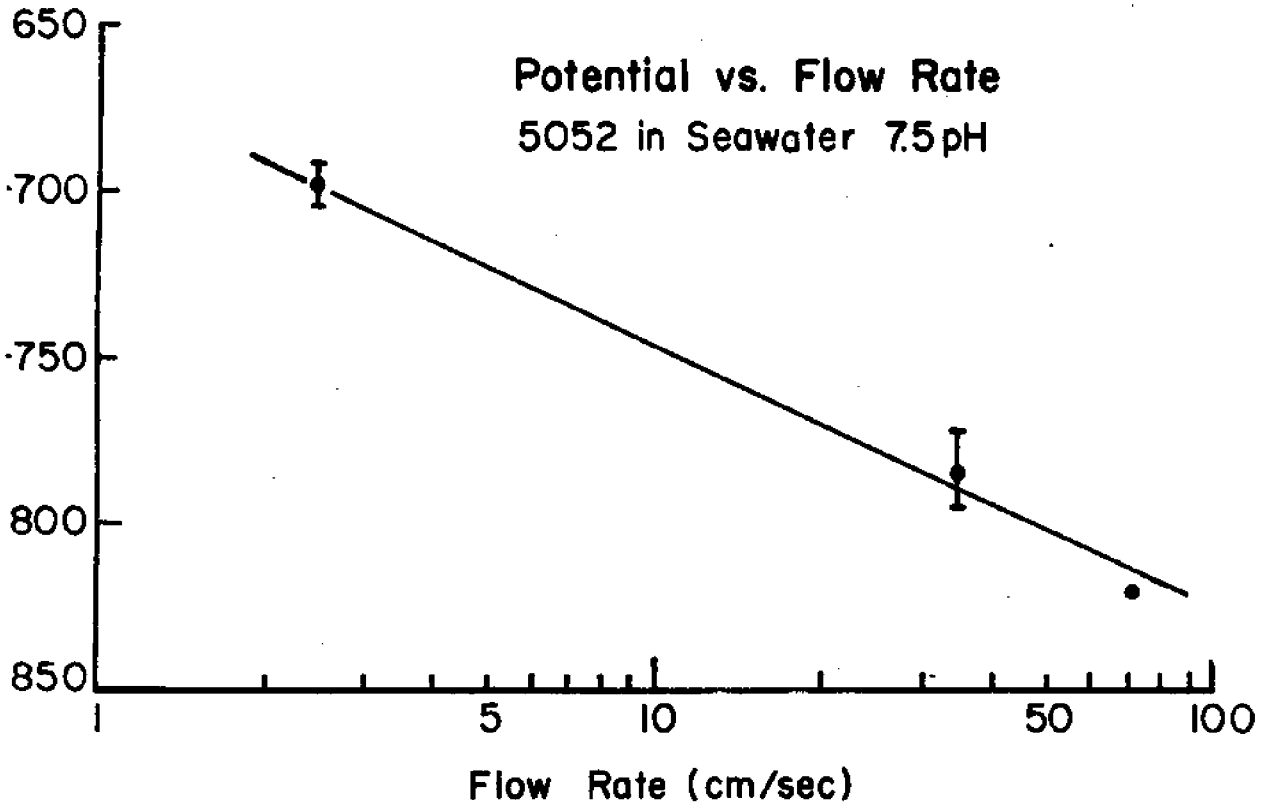

Figure 4.8: Corrosion potential of alloy 5052 in seawater as a function of flow rate at pH 7.5 in the flow through system.

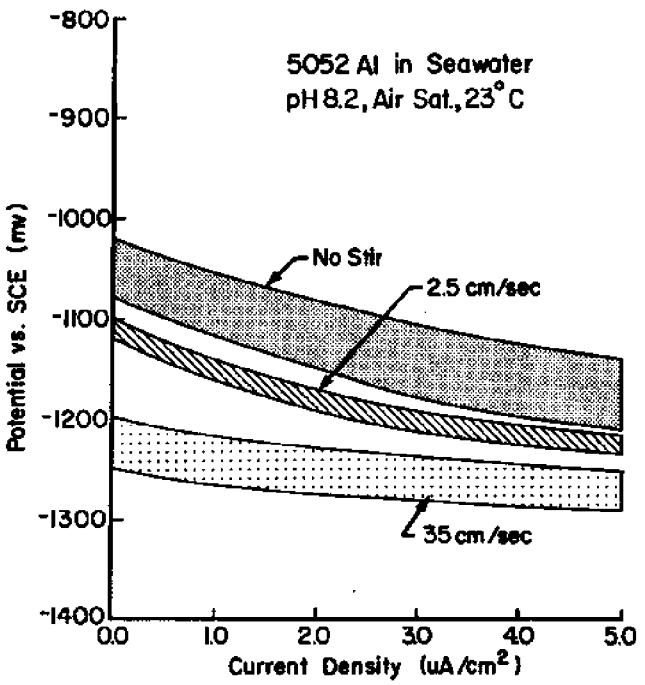

Figure 4.9: Cathodic polarization of alloy 5052 in pH 8.2 seawater in the flow through system as a function of flow rate.

5.0 ACCELERATED LABORATORY TESTS FOR CREVICE CORROSION OF STAINLESS ALLOYS

Part II of the localized corrosion part of the National Corrosion Program is to determine the effects of key factors such as: crevice geometry, surface finish, cathode-to-anode area ratio, seawater temperature and seawater velocity on crevice corrosion of a series of stainless alloys.

Michael Streicher of the Engineering Department at the University of Delaware contributed to this effort by evaluating and developing two types of accelerated laboratory tests for determining corrosion characteristics of 12 stainless alloys.

The data presented in this section is based on the presentation given by Streicher at the workshop and on a paper published in Materials Performance. (14)

Laboratory investigations are being conducted on a range of 46 alloys used in the recent Ocean Thermal Energy Conversion and Navy Seawater immersion test programs at the Francis LaQue Center for Corrosion Technology in North Carolina.

Accelerated laboratory tests have been conducted on most of the alloys tested in the OTEC and Navy programs, Streicher's recent work addresses only 12 alloys common to both programs. Table 5.1 gives the chemical compositions of these alloys in addition to several others used in studying the effect of test parameters.

5.1 Experimental Procedure

The objective of Streicher's work was to compare the results of the laboratory tests with those obtained in natural seawater. In order to accomplish that task a detailed analysis of the data from both series of tests has been done.

The objectives for both experiments were different. The OTEC tests that were reported by Kain (15) were made to obtain data to aid in materials selection for heat exchangers for the OTEC program. This series included 12 commercially available alloys and one experimental alloy with various mill finishes. Close examination of these surfaces showed clear evidence of pitching on all alloys except MONIT which had a mechanically ground finish. The tests were run for 30, 60 and 90 days.

Despite the difference in objectives, there are enough similarities between the two series to make it possible to use data from both for an analysis on the influence of factors such as surface finish, testing time, applied torque and to some extent, alloy composition.

Table 5.1

Analysis of Wrought Stainless Alloys Used in Laboratory Tests

Alloy	Composition, Percent by Weight									
	Cr	Ni	Mo	Mn	C	Si	S	Other		
A.L. 29-4C	28.85	0.79	3.81	0.22	0.012	0.19	0.002	-	0.026 N	0.59 Ti
Monit (Uddeholm)	25.30	4.10	3.80	0.43	0.012	0.31	0.006	0.37 Cu	0.031 P	-
Crucible SC-1	25.56	2.14	2.94	0.20	0.01	0.25	0.004	0.04 Al	0.016 N	0.51 Ti
Ferralium 255 (Cabot)	26.15	5.64	3.20	0.77	0.02	0.37	-	1.75 Cu	0.19 N	0.16 Co
Haynes 20 Mod (Cabot)	21.58	25.52	4.95	0.90	< 0.01	0.49	-	<0.05 Cu	-	0.49 Co
A.L. 6X	20.35	24.64	6.45	1.39	0.018	0.41	0.001	-	0.022 P	-
254 SMO (Avesta)	20.00	17.90	6.10	0.49	0.013	0.41	0.008	0.78 Cu	0.023 P	0.203 N
904L (Uddeholm)	20.50	24.70	4.70	1.46	0.014	0.46	0.005	1.57 Cu	0.028 P	-
Jessop 700	20.70	25.20	4.45	1.65	0.013	0.42	0.008	0.24 Cu	0.28 Nb	-
Jessop 777	20.80	25.60	4.48	1.37	0.023	0.48	0.013	2.18 Cu	0.24 Nb	0.25 Co
Carpenter 329	26.98	4.22	1.39	0.28	0.052	0.39	0.014	0.09 Cu	-	-
Nitronic 50 (Armco)	21.08	13.70	2.28	4.81	0.045	0.47	0.012	-	0.025 P	0.26 N

Above 12 alloys common to both OTEC and Navy programs.

Source: Nagaswami, N., M. Streicher. NACE Conference "Corrosion" '83, April, 1983.

Other tests have been developed to study crevice corrosion of stainless alloys, including immersion tests in natural seawater under various conditions and tests in accelerated laboratory environments. In the latter category, two types of accelerated laboratory crevice tests were selected to study initiation of crevice corrosion:

1. The determination of crevice corrosion temperatures (CCT) in 10% ferric chloride solutions.

2. The determination of crevice corrosion temperatures in synthetic seawater under constant applied potentials.

The research on crevice corrosion of stainless alloys in chloride environments was undertaken to create a rapid laboratory crevice corrosion test to a) rank metals and alloys for service in marine environments, b) investigate the effect of alloying and residual elements in crevice corrosion, c) develop new, more economical alloy compositions having improved resistance in such environments, and d) investigate the mechanism of crevice corrosion.

In order to compare various rapid laboratory test methods with the long term seawater tests, it was necessary to analyze the seawater data for the effect of alloy composition (Cr, Mo, Ni, Mn, Cu, Nb, Ti), surface finish and such test variables as length of testing time and torque on the plastic crevice devices. A method was developed for ranking alloys based on a Crevice Corrosion Index (CCI). CCI = S x D, where S is the number of panel faces showing crevice attack in a group of at least 3 panels (6 faces), and D is the maximum depth of attack measured on these faces. S is a measure of initiation and D a measure of growth of crevice corrosion. Details of the CCI are presented in the aforementioned Materials Performance May 1983 article. (16)

Composition

Copper. Copper, which is present between 1.6 to 3.3% in some of the alloys tested, had a significant effect on crevice corrosion. It appears to increase the resistance to breakdown of the oxide films formed during mill processing. But when this film is removed by polishing to a 120 grit finish or by cutting and shearing at edges, Cu promotes initiation and growth of crevice attack. The reason is probably galvanic action by Cu in the acid chloride environment of crevices.

Manganese and Nitrogen. Manganese, when present in concentrations greater than about 4%, together with about 0.25N or more, reinforces the effect of Mo in retarding the growth of crevice attack. For example, AISI 216 (8Mn-2.5Mo-6Ni-0.35N) was found to be superior to 316 and 317 SS (2.4 to 4.2 Mo).

Titanium and Niobium. Titanium, added as a stabilizer for C and N, seems to enhance resistance to crevice corrosion, while Nb has the opposite effect.

Correlation with Service

There is a need to correlate the results obtained in the crevice tests in quiescent, filtered seawater at 30°C with various types of service exposures in marine environments. One such correlation is available for the old and new Sea Cure alloys. It has been found that the old Sea Cure, which showed a slight degree of susceptibility in both the OTEC and Navy tests, was also attacked ("slight pitting and crevice corrosion") in service in several condensers on power plants using brackish water. Thus, in this case, the severe OTEC crevice test did detect a degree of susceptibility which also made this alloy vulnerable in the one kind of service which is of greatest importance for this alloy.

Available data suggest that rapidly flowing, unfiltered sea water at temperatures other than 30 C may provide a less severe corrosion environment than that used for the OTEC and Navy tests. Cathodic protection, deliberate or incidental (by contact with carbon steel) can also effectively reduce crevice attack on stainless steels. These factors must be taken into account in the application of data from the ranking lists developed in this analysis.

Use of Crevice Corrosion Index

The ranking methods used in this analysis may be of some use even before more extensive correlations with marine service become available. If a ranking table based on the CCI is supplemented with two other columns, the combination can serve as an aid in the selection of materials. These other columns would be lists of available mill forms (tubes, sheet, plate) for each alloy and unit prices for these forms. To select a replacement material for an alloy that has failed in service, this list might then be used to review alloys which have lower CCI values than the alloy that failed and, amongst these, to select the alloy nearest the top of the list for which the mill forms have the most favorable price.

Test Conditions

The findings of this investigation also provide guidance for improvements in an ASTM crevice corrosion test procedure. The recommended conditions for tests of maximum severity are:

1. Surface finish - 120 grit
2. Torque - 75 in. lb on plastic washers (crevice devices) (perhaps with periodic reapplication of torque to promote more constant crevice conditions).

3. Time - 30, 60, 90 and 120 days, depending on the alloy
4. Number of panels - 12
5. Quiescent conditions with filtration
6. Analysis of results by the number of sides or panels attacked, the maximum depth of attack, and by application of the CCi described here
7. For comparison of two or more alloys, the testing program must be the same; this includes the number of panels, testing times, torque, surface finish, temperature, and seawater conditions

New Test Series

To provide direct experimental support for some of the conclusions derived from the analysis of the two test programs, several new series of crevice corrosion tests are needed, not only on commercially available alloys, but also on some compositions specifically designed to reveal the effect of alloying elements. The following subjects are suggested for some new crevice corrosion tests in natural, filtered seawater:

1. Investigate "relaxation" of Delrin with time and, if necessary, devise a method of periodic reapplication of the initial level of torque without removal of the specimen from the water.

2. Using the original and the new method for applying torque on the crevices, determine the number of panels needed to provide reproducible results. Do the more constant levels of torque provide reliable data on the effect of testing time and levels of torque and, therefore, make it possible to reduce the number of panels which must be tested?

3. Select series of alloys to more precisely define: the minimum requirements for Cr and Mo in iron; the effect of Ni on the requirements for Cr and Mo; the effect of Cu on initiation and growth of crevice attack; the effect of Ti and NB; and crevice growth in Fe-Cr-Mo ferritic SS to determine whether it differs from alloys with 8% or more Ni.

5.2 Conclusions and Perspectives on Ranking of Stainless Alloys

Among the most important aspects of any corrosion test are the criteria selected for proper evaluation of the test results. Because the crevice corrosion process is clearly separated into initiation and propagation phases, test data should be analyzed to determine relative alloy resistance to each stage of the process. The separate treatment of the two phases is theoretically credible since the mechanisms of crevice corrosion initiation and propagation are different. As such, various factors can be expected to influence each process differently (such as the previously discussed effects of initial crevice gap).

This clear separation of the crevice corrosion initiation and propagation behavior of alloys is particularly important from a practical viewpoint. A designer or engineer can select an alloy which may be subject to crevice corrosion initiation under certain conditions but which has an acceptably low degree of propagation. Any treatment of data which combines the two phases allows no such delineation of alloy behavior and literally forces an engineer into a go/no-go decision on materials selection.

6.0 THE EFFECT OF ADSORBED ORGANIC AND BACTERIAL FILMS ON THE SETTLEMENT AND ADHESION OF MARINE LARVAE

University of Delaware PhD candidate James Mihm presented the results of his thesis work on the effect of adsorbed organic and bacterial films on the settlement and adhesion of marine larvae.

Understanding the sequence of steps in bioattachment to substrata is fundamental to studying marine larvae substrata selection. The sequence of larval attachment is a 4-step process. Step 1 represents the clean substratum immediately after it is immersed in seawater. Within 1 to 5 seconds dissolved organics begin to adsorb on the substratum, beginning step 2. Step 3 occurs 2 to 4 hours after immersion, when bacteria begin to adhere and colonize the substratum. Bacteria are attracted to the substratum to exploit the adsorbed organic macromolecules, which serve as a nutrient resource. Within 24 hours after immersion, larvae of macroinvertebrate fouling organisms begin to attach to the substratum, which is designated as step 4. These fouling organisms include bryozoans, mussels, barnacles, and oysters.

In this study the larvae of the common fouling bryozoan, Bugula stolonifera, were used in settlement experiments. They are colonial organisms comprised of many small individuals living in an arboreal colony. The colonies grow to approximately 10 cm high and 5 cm wide. Each individual adult produces a free swimming larva that will attach to a solid surface and grow into an adult colony. Once the larvae settle they permanently attach to the substratum and cannot change their position. Thus it is very important for the larvae to choose an environment suitable for the success of the adult colony. Because of their important role, the larvae are equipped with a variety of sensory organs to ensure selection of a proper environment (Figure 6.1). Because the larval eye spot is light sensitive the larvae swim toward the bright surface water when they are first released. After a brief free-swimming phase, the larvae swim away from light and return to the bottom area for settlement. Once the larvae locate a solid surface they beat their ciliated tuft across the surface and then up through their ciliated groove. It is believed that the larvae are testing the chemical properties of the surface and the associated adsorbed organics.

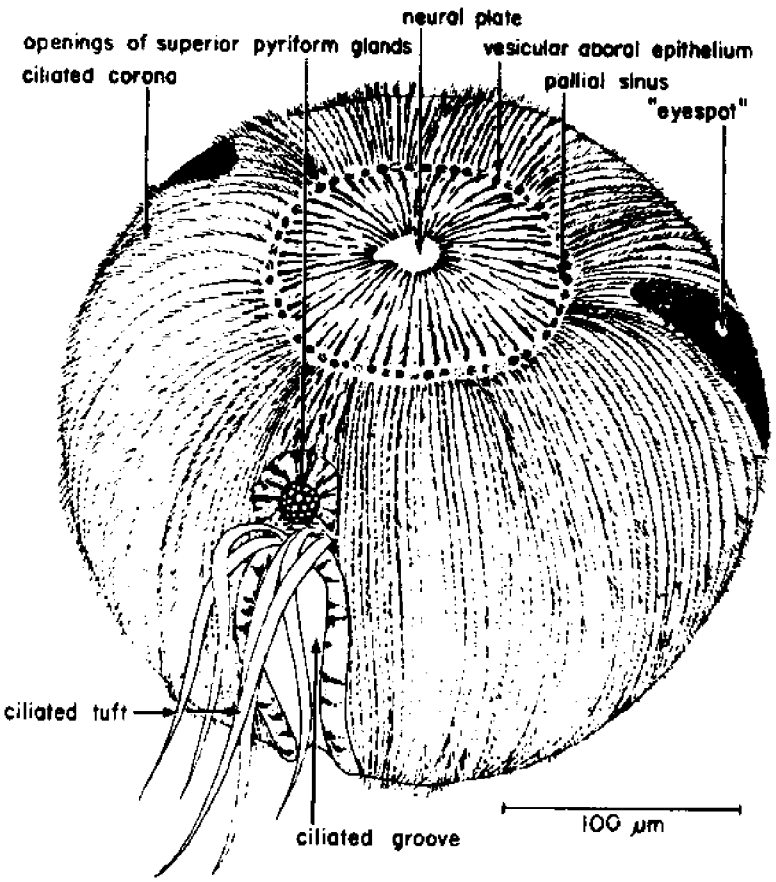

Figure 6.1: Exterior Anatomy of Bryozoan Larvae, Bugula neritina.

Source: Woollacott, R.M. and R.L. Zimmer (1971) Attachment and Metamorphosis of the Cheilo-ctenostome Bryozoan, Bugula neritina (Linne) J. Morphol. 134, 351-387.

The purpose of this research was to determine what factors control settlement preferences of the larvae with respect to the adsorbed organic and bacterial films which form on submerged surfaces. Another objective was to determine the adhesive strength of the larvae after they permanently attach to the test substrata.

Table 6.1 lists the seven substrata that were used in these experiments. Substrata were chosen on the basis of their critical surface tension (an approximation of the surface energy), and the consistency of their surface texture. Larval settlement tests were conducted on these substrata, simulating steps 1, 2, and 3 of the bioadhesion process.

TABLE 6.1

Experimental Substrata	CST
Glass	46
Polystyrene (PS)	33
Polyethylene (PE)	31
Polyvinylfluoride (PVF)	28
Polyvinylidenefluoride (PVF_2)	25
FEP Teflon (6000-L)	23
Polytetrafluoroethylene (TFE)	18

Note: Experimental Materials used to determine larval settlement preferences for the Bryozoan, Bugula stolonifera.

The results of the settlement preference tests are given in Table 6.2. On clean substrata, representing step 1, larval settlement was high on all materials except glass and PVF2. After a 24-hour natural seawater organic film had adsorbed on the substrata (step 2), low settlement occurred on glass, 6000-L and the TFE, which high settlement occurred on the remaining substrata. This settlement pattern also was evident in the 336-hour natural seawater organic film formation time.

Table 6.2

Percent Settlement of Bugula stolonifera Larvae on Materials that are Clean, with an Organic Film or with a Bacterial Film (in 24 hours)

	Clean	Organic Films		Bacterial Films	
		24hr	336hr	24hr	336hr
Glass	9	18	5	73	88
PS	80	76	87	10	87
PE	82	73	89	76	89
PVF	89	87	91	89	87
PVF2	7	66	87	78	90
6000-L	79	16	3	19	87
TFE	83	15	5	79	89

When comparing settlement on the clean substrata and the same substrata with an organic film the larvae exhibited some preference reversals. Larvae did not settle on clean PVF2 but did settle once the organic film had formed. The opposite was seen with 6000-L and TFE. High settlement occurred when these substrata were clean, while low settlement followed after the organic films had formed.

A possible explanation for the settlement preference changes is that there is a difference in the type of organic molecules being adsorbed on the substrata. Since these substrata are chemically different, they might offer different binding sites for the organic molecules in seawater. Also, conformational changes, occurring when the organics are adsorbed on the substrata, may affect larval settlement.

To further define the relationship between larvae settlement preferences and the organic conditioning films, dissolved organics in seawater were fractioned into four categories based on the molecular weights and size of the organic molecule (Table 6.3).

TABLE 6.3

Natural Seawater Organic Fractions

A	< 1000 daltons
B	< 5000 daltons
C	< 10000 daltons
D	< 1000 > 10000 daltons

Molecular Weight Fractions of the Dissolved Organic Macromolecules in Natural Seawater Using Ultrafiltration.

The effects of the organic fractions on settlement can be compared by plotting the percent settlement of larvae versus the critical surface tension of each substratum. Figure 6.2 illustrates the percent larval settlement on substrata filmed with either a 1000 dalton or 5000 dalton molecular weight organic film, and settlement on clean substrata. The data indicate that larval settlement is approximately equal on the clean substrata and on substrata filmed with the two smaller molecular weight fractions. These results indicate that the smaller molecular weight organics do not influence the larvae's selection of substrata.

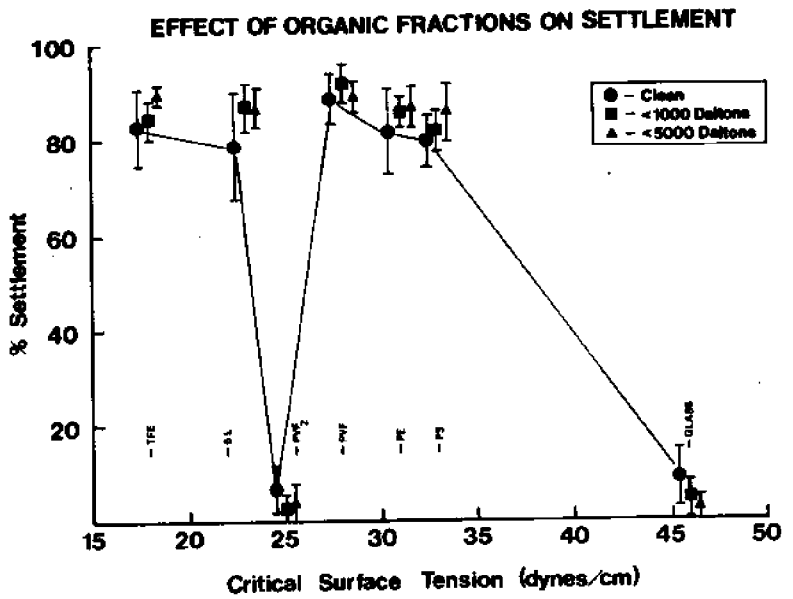

Figure 6.2: Percent settlement of Bugula stolonifera larvae on materials with <1000 and <5000 MW organic films compared to clean materials.

Figure 6.3 shows the percent settlement of larvae on substrata with films of molecular weight fractions of < 10,000 daltons, > 10,000 daltons, compared to a 24-hour natural seawater organic film. The data find that there is little difference between larvae settlement on either of the molecular weight fractions or the natural seawater organic film, indicating that the larger molecular weight fractions indeed play an important role in conditioning the substratum for larval settlement. Also, a wide size range of organics seem to be capable of conditioning the substrata, resulting in increased or decreased settlement.

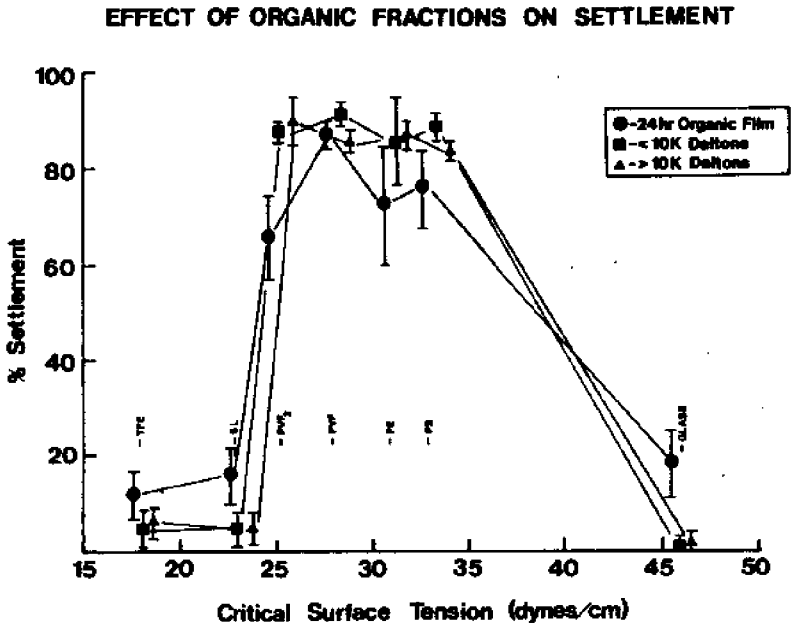

Figure 6.3: Percent settlement of Bugula stolonifera larvae on materials with < 10,000 and > 10,000 MW films compared to a natural seawater organic film.

The larvae were then tested at the third step in the bioadhesive sequence, after bacteria have adsorbed on the substrata. Bacteria begin to attach to the substrata after two hours of immersion. The numbers of bacteria and the amounts of bacterial extracellular polysaccharides continue to increase with increased immersion times.

Table 6.2 depicts the settlement preferences of the larvae on substrata after 24-hour and 336-hour bacterial films had formed. When a 24-hour bacterial film formed on substrata, larval settlement preferences changed compared to substrata with a natural seawater organic film. Low settlement occurred on PS and 6000-L, while high settlement occurred on the remaining substrata. However, after a 336-hour bacterial film formed on the substrata, larval settlement was high on all substrata. When compared to settlement on substrata filmed with natural seawater organic films there were also settlement reversals. Larvae settlement changed from low to high on glass and TFE, and from high to low settlement on PS.

To further assess the effects of bacteria on settlement preferences, single-species bacterial films were adsorbed on each substrata. The bacteria used (Table 6.4) were received from Dr. R. Colwell at the University of Maryland.

TABLE 6.4

% SETTLEMENT ON SINGLE SPECIES BACTERIAL FILMS

	Bacterial Types				
	A	B	C	D	E
Glass	89	90	89	2	2
PS	92	86	90	1	3
PE	89	91	91	2	3
PVF	91	90	92	3	3
PVF_2	88	86	91	3	2
6000-L	89	89	93	2	1
TFE	91	90	93	2	1

Percent settlement of Bugula stolonifera larvae on materials with single-species bacterial films.

Note: Listed below are the five bacterial species used to form the single-species bacterial films on substrata.

A = Vibrio parahaemolyticus
B = Vibrio aldinolyticus
C = Hyphomicrobium sp.
D = LST-1 undescribed
E = Pseudomonas sp.

Larval settlement preferences on substrata with single-species films showed that the type of bacteria will either inhibit or stimulate settlement (Table 6.4). It is interesting to note that the effect of the bacteria on settlement is independent of the substratum type. These results are similar to settlement patterns on natural bacterial films formed after 336-hour immersion times in that settlement was also independent of the substratum type.

TABLE 6.5

Percent Settlement on Bugula Stolonifera Larvae on Materials that are Clean, with an Organic Film or with a Bacterial Film (in 24 hours)

	Clean	Organic Films		Bacterial Films	
		24hr	336hr	24hr	336hr
Glass	9	18	5	73	88
PS	80	76	87	10	87
PE	82	73	89	76	89
PVF	89	87	91	89	87
PVF2	7	66	87	78	90
6000-L	79	16	3	19	87
TFE	83	15	5	79	89

To explain the settlement patterns on the 24-hour and 336-hour natural bacterial films, and the single-species bacterial films, one theory states that as the length of the immersion times increases, bacterial populations change on the substrata. After a 336-hour immersion time there are similar populations on all substrata, showing results similar to those on the single-species films.

Strength of Adhesion

The adhesive strength of individual larva was measured by recording the water velocity flowing through a pipette aimed at the attachment disc of the larva. Velocity was then reported as a flow rate per second.

The adhesive strength of larvae on clean substrata decreased along with the substrata's critical surface tension (Figure 6.4). However, the adhesive strength increased on clean TFE, which has the lowest critical surface tension. This increase could have been due to the slightly greater surface roughness of the TFE. To test if surface roughness could produce an increase in the adhesive strength, a piece of 6000-L was roughened with 400 grit sand paper. When the adhesive strength of larvae was measured on this substrata, it increased significantly. Thus, the increased adhesive strength on the TFE was likely due to its surface roughness.

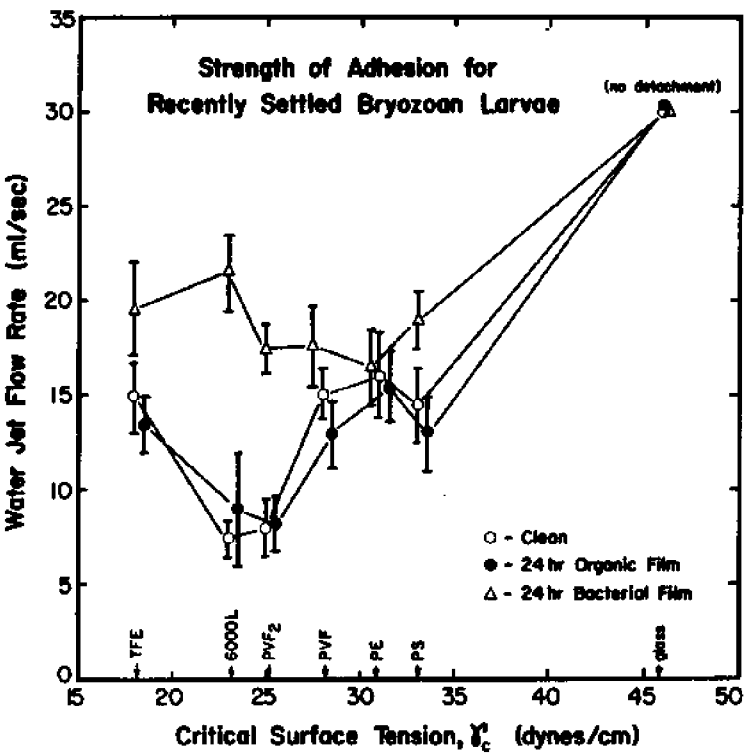

Figure 6.4: Relative adhesive strength of recently settled bryozoan larvae on 7 non-toxic substrata when clean, and with organic or bacterial film.

The reduced adhesive strength that occurs with a decrease in the substratum critical surface tension is consistent with adhesive theory. This theory states that the best adhesive joints will be formed when the adhesive spreads completely over the surface. The experimental data indicate that larval adhesives will spread more completely on substrata with higher critical surface tensions, and thus show greater adhesive strength values on these substrata. It should also be noted that this method could not remove the larvae that had settled on the glass substratum regardless of the film types. Glass has the greatest critical surface tension of the substrata tested and would be expected to show the greatest adhesive strength values.

After a 24-hour natural seawater organic film had formed on the substrata the adhesive strength was not significantly different than that on clean substrata. Since the adsorbed organics do not affect the adhesive strength, it can be theorized that larval adhesives can displace the adsorbed organics. The adhesive joint would then be formed between the adhesive and the substratum, as it is on a clean substratum.

The adhesive strength on substrata with a 24-hour bacterial film is significantly greater than the clean or organically filmed substrata, except for PE which showed no change. These data demonstrate that bacteria highly influence the adhesive strength of the larvae because the adhesive joint is now formed between the bacterial cell wall and the larval adhesive. This theory accounts for both the increase in the adhesive strength and the similar adhesion values for all substrata. It is interesting to note that the critical surface tension of the bacterial cell walls may be similar to the critical surface tension of PE since the adhesion values are similar. A combination of critical surface tension and surface roughness could also account for the similar adhesion values.

Summary

These experimental results indicate that bacteria play an important role in both conditioning the substrata for larval settlement, and influencing the adhesive strength of larvae. A practical approach to biofouling prevention should concentrate on limiting the attachment and growth of bacteria, as opposed to the toxic control of larger macroinvertebrates. It may also be conceivable to develop non-toxic substrata or coatings that will be more easily cleaned because of bacterial control.

7.0 REFERENCES

1. Dexter, Stephen, W. Hartt, Sea Grant Program on Marine Corrosion Final Report, Volume One - Technical Summary, University of Delaware, August 1984.

2. Dexter, S., N. Moettus, K. Lucas, "On the Mechanism of Cathodic Protection," Paper presented at NACE Conference Corrosion '84, April 2-6, 1984, New Orleans, LA.

3. Mears, R., Brown, R. Trans. Electrochem. Soc., Vol. 74, p. 519, 1938.

4. Hoar, T.P., J. "Electrodepositors," Tech. Soc., Vol. 14, p. 33

5. LaQue, F.L., May, T.P., "Proceedings, 2nd International Congress on Metallic Corrosion, National Association of Corrosion Engineers, p. 789, 1965.

6. & 7. Dexter, S., N. Moettus, K. Lucas, "On the Mechanism of Cathodic Protection," Paper presented at NACE Conference Corrosion '84, April 2-6, 1984, New Orleans, LA.

8. Culberson, C., "Effect of Seawater Chemistry on the Formation of Calcareous Deposits," Paper #61 presented at NACE Conference "Corrosion '83", April 18-22, 1983.

9. Ibid.

10. Linskey, M., "Corrosion of Aluminum in Seawater," MIT Sea Grant Marine Industry Collegium Draft Opportunity Brief #31, December 1, 1982.

11. Dexter, S. et al. "Effect of Water Chemistry and Velocity of Flow on Corrosion of Aluminum." Paper presented at NACE Conference "Corrosion '83", April 18-22, 1983.

12. Ibid.

13. Gehring, G.A. Jr., M.A. Peterson, Corrosion, Volume 37, p. 232 1981.

14. Streicher, Michael, "Analysis of Crevice Corrosion Data from Two Seawater Exposure Tests on Stainless Alloys." Materials Performance, Vol., 22, No. 5, pp. 37-50, May 1983.

15. Kain, R.M. "Crevice Corrosion & Metal for Concentration Cell Corrosion Resistance of Candidata Materials for OTEC Heat Exchangers, Parts I & II," LaQue Center for Corrosion Technology, Inc., U.S. Department of Energy Contract #31-109-38-4974, May 1981.

16. Streicher, Michael, "Analysis of Crevice Corrosion Data from Two Seawater Exposure Tests on Stainless Alloys." Materials Performance, Vol., 22, No. 5, pp. 37-50, May 1983.

8.0 APPENDIX

MIT Marine Industry Collegium Workshop #37
March 13, 1984
Part III: Marine Corrosion & Biofouling
John Clayton Hall, Room 125
University of Delaware, Newark, Delaware

AGENDA

7:30 Registration - John Clayton Hall Lobby
Continental Breakfast - Room 125

8:45 Welcome
Dr. Carolyn Thoroughgood - Executive Director, University of Delaware, Sea Grant Program

8:50 Introduction
Margaret Linskey, Assistant Manager, MIT Marine Industry Collegium

9:00 Overview of Marine Corrosion Research at University of Delaware
Sea Grant Corrosion Program Chairman, Dr. Stephen Dexter, College of Marine Studies

9:15 Mechanism of Cathodic Protection and its Effect on Marine Structures
Dr. Stephen Dexter, Associate Professor of Marine Materials Science
College of Marine Studies

10:00 The Effect of Seawater Chemistry on the Formation of Calcareous Deposits During Cathodic Protection
Dr. Charles Culberson, Associate Professor of Oceanography
College of Marine Studies

11:00 Accelerated Laboratory Tests for Crevice Corrosion of Stainless Alloys in Seawater
Dr. Michael Streicher, Research Professor, College of Engineering

12:00 Lunch: Dining Room 101B

1:15 The Effect of Water Chemistry & Velocity of Flow on Corrosion of Aluminum and Aluminum Alloys
Dr. Stephen Dexter, Associate Professor of Marine Materials Science
College of Marine Studies

2:00 The Effect of Adsorbed Organic Films on Settlement and Adhesion of Marine Larvae
James Mihm, PhD Candidate in Marine Biology, College of Marine Studies

3:00 Laboratory Tours: Lobby of Clayton Hall to meet Shuttle Bus